Experimental evolution in maize with replicated divergent selection identifies plant-height associated SNPs

Mila Tost[1,2], Cathy Westhues[1,2], Ginnie Morrison[3], Dietrich Kaufmann[1] and Timothy Beissinger[1,2,*]

[1]Department of Crop Science, Division of Plant Breeding Methodology, University of Goettingen, Carl-Sprengel-Weg 1, Goettingen, 37075, Germany

[2]Center for Integrated Breeding Research, University of Goettingen, Carl-Sprengel-Weg 1, Goettingen, 37075, Germany

[3]University of Missouri, Division of Biological Sciences, 105 Tucker Hall, Columbia, MO, 65211, USA

[*]**Corresponding author:** Timothy Beissinger (timbeissinger@gmail.com)

Mila Tost (mila.tost@uni-goettingen.de)

Running title: Replicated experimental evolution maize

Key words: Experimental evolution, Population genetics, maize, selection signature mapping, plant height

Abstract

Experimental evolution studies are common in agricultural research, where they are often deemed "long term selection". These are often used to perform selection mapping, which involves identifying markers which were putatively under selection based on finding signals of selection left in the genome. A challenge of previous selection mapping studies, especially in agricultural research, has been the specification of robust significance thresholds. This is in large part because long term selection studies in crops have rarely included replication. Usually, significance thresholds in long term selection experiments are based on outliers from an empirical distribution. This approach is prone to missing true positives or including false positives. Under laboratory conditions with model species, replicated selection has been shown to be a powerful tool, especially for the specification of significance thresholds. Another challenge is that commonly used single-marker based statistics may identify neutral linked loci which have hitchhiked along with regions that are actually under selection. In this study, we conducted divergent, replicated selection for short and tall plant-height in a random mating maize population under real field conditions. Selection of the 5% tallest and shortest plants was conducted for three generations. Significance thresholds were specified using the false discovery rate for selection (FDRfS) based on a window-based statistic applied on a statistic leveraging replicated selection ($F_{ST}Sum$). Overall, we found 3 significant regions putatively under selection. One region was located on chromosome 3 close to the plant-height genes *Dwarf1* and *iAA8*. We applied a haplotype block analysis to further dissect the pattern of selection in significant regions of the genome. We observed patterns of strong selection in the subpopulations selected for short plant height on chromosome 3.

Introduction

The purpose of experimental evolution studies is to understand how populations evolve in response to a selective pressure (Janick, 2010a, 2010b). In agricultural research, they are commonly employed and often deemed "long term selection" studies (Dudley and Lambert, 2010; Moose, Dudley and Rocheford, 2004, Beissinger *et al.,* 2014). For instance, the Illinois long-term selection experiment for maize protein content began in 1896 at the University of Illinois and has been conducted ever since (Moose, Dudley and Rocheford, 2004; Dudley and Lambert, 2010). Experimental evolution studies are also common in model organisms like mice (Firman *et al.*, 2015; Palma-Vera et al., 2022), *Drosophila melanogaster* (Phillips *et al.*, 2016; Mallard, Afonso and Teotónio, 2023), *E. coli* (Barrick *et al.*, 2009; Card *et al.*, 2021), *Mimulus guttatus* (monkey flowers) (Angert, Bradshaw Jr and Schemske, 2008; Tusuubira and Kelly, 2024), and yeast (Payen *et al.*, 2016; Linder *et al.*, 2021). Early experimental evolution studies focused on the evolution of phenotypes alone, but now sequencing technologies allow researchers to study the effect of selection at the DNA level (Burke *et al.,* 2010; Parts *et al.*, 2011; Orozco-terwengel *et al.,* 2012; Remolina *et al.,* 2012).

Many experimental evolution studies in model organisms work with replicates (Teotónio and Rose, 2000; Phillips *et al.*, 2020; Mallard, Afonso and Teotónio, 2023). These studies are often referred to as Evolve & Resequence (E&R) experiments (Phillips *et al.*, 2020). E&R experiments commonly employ pooled sequencing of the different subpopulations (Orozco-terWengel *et al.,* 2012; Long *et al.*, 2015; Phillips *et al.*, 2020). In agricultural species, experimental evolution studies that leverage replicated selection populations are exceedingly rare (Dudley and Lambert, 2010, Beissinger *et al.*, 2014; Kumar *et al.*, 2021). On the other hand, replication plays a very

important role in E&R studies because it can help to identify putatively selected sites and differentiate those from sites caused by drift (Turner and Miller, 2012; Otte and Schlötterer, 2020; Linder *et al.*, 2021; Lai *et al.*, 2024). This assumes that selection is repeatable, while randomly acting forces like drift are not (Burke, Liti and Long, 2014; Phillips *et al.*, 2020, Otte and Schlötterer, 2020; Schlötterer, 2023).

Genetic drift is a complicating factor in experimental evolution studies because it can be difficult to differentiate from selection (Krimbas and Tsakas, 1971; Turner *et al.*, 2011; Hirsch *et al.*, 2014). This is a recurring challenge in unreplicated selection mapping studies, because without replicating the evolutionary process, no amount of sampling can estimate the variability associated with genetic drift (Krimbas and Tsakas, 1971; Barghi, Hermisson and Schlötterer 2020, Kumar *et al.*, 2021; Lai *et al.*, 2024). The variability introduced by genetic drift depends on population size and the number of generations of selection (Baldwin-Brown, Long and Thornton, 2014; Kessner and Novembre, 2015; Barghi, Hermisson and Schlötterer, 2020). Replicated selection populations can help differentiate neutral loci subject to drift alone, from putatively selected loci (Kofler and Schlötterer, 2014; Barghi *et al.,* 2019; Linder *et al.,* 2021). Replicates can be analyzed to calculate a null expectation and to derive an approximation of the number of false positive observations in the experiment (Turner and Miller, 2012; Lai *et al.*, 2024).

In previous experimental evolution studies on crops, significance thresholds for identifying signals of selection were frequently derived based on outlier quantiles of the empirical distribution (e.g. Wang *et al.*, 2018; Ayalew *et al.*, 2020, Semagn *et al.*, 2021). This assumes that

69 selection is a locus-specific force; putatively selected loci should be found at the tail of the
70 empirical distribution (Akey *et al.*, 2002; Akey, 2009). Drift is assumed to act uniformly genome-
71 wide, so drifting loci dictate the bulk of the empirical distribution (Akey *et al.*, 2002; Akey, 2009).
72 However, it has been recognized for a very long time that outlier-based thresholds are arbitrary
73 (Akey *et al.*, 2002; Akey, 2009).
74
75 For this study, we performed replicated divergent selection for plant height on a random mating
76 maize population for three generations. Plant height is an ideal model trait because it is highly
77 heritable and highly polygenic (Pfeiffer *et al*., 2014, Mazaheri *et al.,* 2019). We replicated
78 selection on four subpopulations, two of which were selected for tall plant height and two
79 which were selected for short plant height. Each subpopulation was maintained with a
80 population size of approximately 5,000 individuals. Every generation, we selected the 5% tallest
81 or shortest plants (~250 plants). The truncation threshold of 5% tallest or shortest plants was
82 calculated based on 96 randomly sampled plants from each subpopulation (in total 384 plants).
83 The 384 randomly sampled plants from the fourth generation were also used for genotyping-by-
84 sequencing (GBS) to conduct selection mapping.
85
86 Regions corresponding to selection can be quite large and contain neutral linked loci (Tobler *et*
87 *al.*, 2014; Franssen, Barton and Schlötterer, 2016; Barghi and Schlötterer, 2019). Single marker-
88 based statistics like F_{ST} are prone to identify neutral loci that have hitchhiked along with those
89 that are under selection (Tobler *et al.*, 2014; Franssen, Barton and Schlötterer, 2016). Several
90 experimental evolution studies have additionally investigated reconstructed haplotype blocks to

disentangle the complex pattern of linkage (Michalak *et al.*, 2019; Otte and Schlötterer, 2023; Chen, Pelizzola and Futschik, 2023). These investigations showed that often a large number of putatively significant sites corresponds to only a small number of significant haplotype blocks (Michalak *et al.*, 2019; Chen, Pelizzola and Futschik, 2023). Therefore, we applied a cubic smoothing spline approach to identify window boundaries and corresponding values of a statistic denoted as "*Wstat*" for selection regions (Beissinger *et al.*, 2015). This procedure may also reduce the inflation of observations due to linked loci (Barghi and Schlötterer, 2019; Chen, Pelizzola and Futschik, 2023). Finally, we generated significance thresholds based on Turner and Miller's (2012) false discovery rate for selection (FDRfS), but instead of using single marker observations we calculated the FDRfS based on our previously defined regions. Finally, to assess the utility provided through replication, we compared these replication-based significance thresholds to those generated from the empirical distribution of *Wstat*. Additionally, we phased our data and investigated the haplotype blocks in the regions putatively under selection.

Material and methods

Plant materials and experimental design

The Shoepeg population is a maize Southern dent landrace population (Doebley *et al.*, 1988), which was collected as open-pollinating variety in 1960 in Missouri, USA. We ordered Shoepeg material from the National Plant Germplasm System as accession PI 269743 (U.S. National Plant Germplasm System, 2021). Seeds were greenhouse-propagated to generate our starting population for selection. The formation of the Shoepeg experimental evolution population and results preceding the first generation of selection are described in Gyawali *et al.* (2019). To

113 summarize, in 2016 the Shoepeg population was divided into four subpopulations, each
114 consisting of approximately 5000 plants which were allowed to open-pollinate. In each
115 subpopulation, plant height was measured (Figure 1). In total, 384 (96 x 4) individual plants out
116 of approximately 20,000 (5000 x 4) plants were measured across all four subpopulations (Figure
117 1). Based on these plant height measurements, a truncation threshold corresponding to
118 approximately the 5% shortest or tallest plants was calculated for each subpopulation (Figure 1)
119 (Gyawali *et al.*, 2019). Two subpopulations were selected for short plants, and two were
120 selected for tall plants. The ~5% shortest or tallest plants from each subpopulation were
121 harvested as females to generate the next generation (Figure 1) (Gyawali *et al.*, 2019).
122
123 This procedure was repeated in 2017 and 2018 (Figure 1). Ultimately, we generated four
124 experimentally evolved subpopulations, two comprised of short-selected plants and two
125 comprised of tall-selected plants (Figure 1). The populations were grown again in 2020 and plant
126 height was measured for 96 randomly-chosen representative plants in each subpopulation (in
127 total 384 plants). Additionally, tissue was collected from the same 384 plants for genotyping
128 (Figure 1).
129

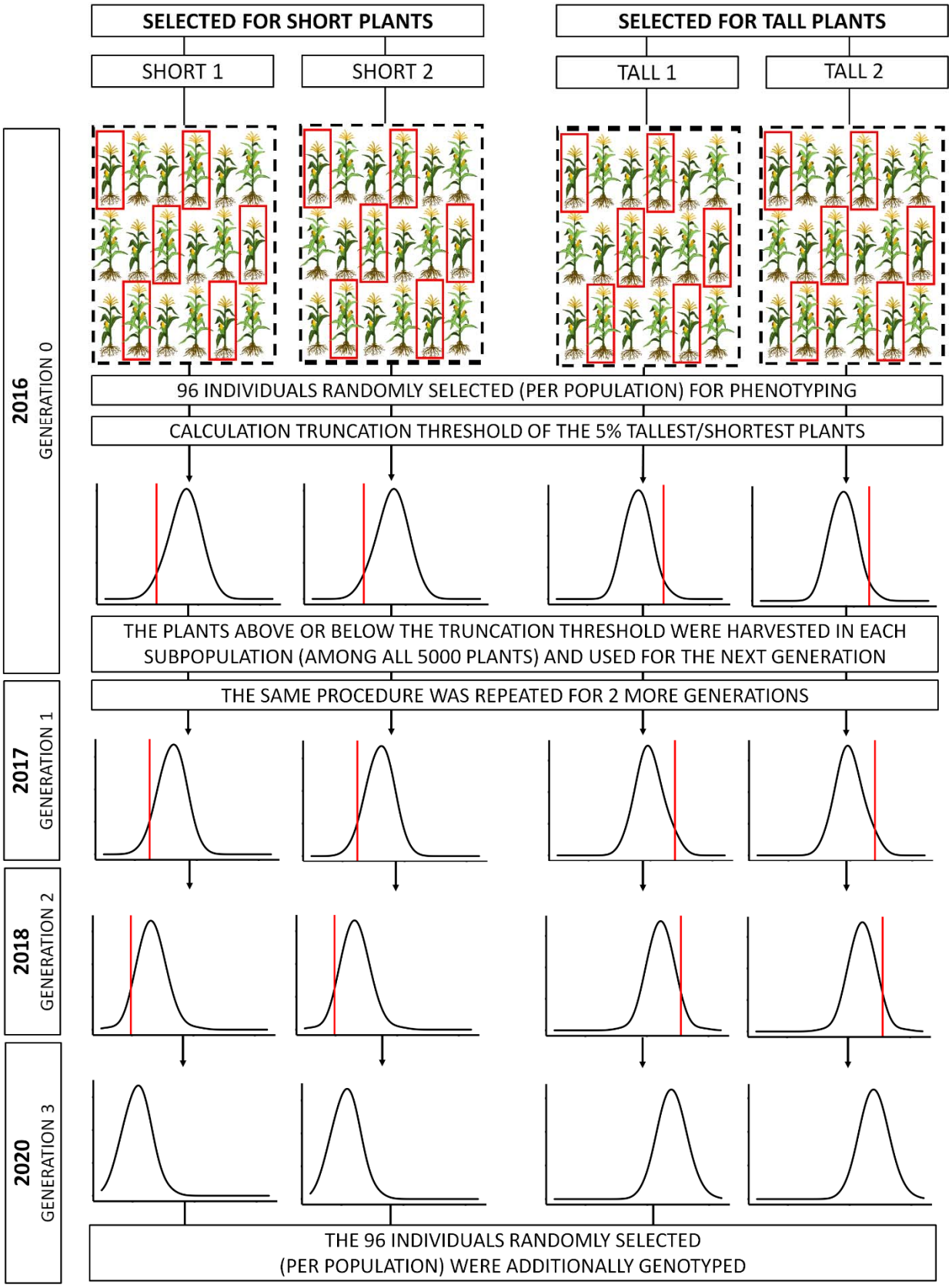
SELECTED FOR SHORT PLANTS
SELECTED FOR TALL PLANTS
SHORT 1
SHORT 2
TALL 1
TALL 2
2016
GENERATION 0
96 INDIVIDUALS RANDOMLY SELECTED (PER POPULATION) FOR PHENOTYPING
CALCULATION TRUNCATION THRESHOLD OF THE 5% TALLEST/SHORTEST PLANTS
THE PLANTS ABOVE OR BELOW THE TRUNCATION THRESHOLD WERE HARVESTED IN EACH SUBPOPULATION (AMONG ALL 5000 PLANTS) AND USED FOR THE NEXT GENERATION
THE SAME PROCEDURE WAS REPEATED FOR 2 MORE GENERATIONS
2017
GENERATION 1
2018
GENERATION 2
2020
GENERATION 3
THE 96 INDIVIDUALS RANDOMLY SELECTED
(PER POPULATION) WERE ADDITIONALLY GENOTYPED

130

Figure 1: Simplified scheme for the development of subpopulations selected in divergent directions with their replicates for the three generations of selection. The subpopulations short 1 and 2 were selected for short plant height and the subpopulations tall 1 and 2 were selected for tall plant height.

Every year after the first, the subpopulations were grown in isolated fields at least 200 m apart and away from any other maize to avoid contamination via cross-pollination (Nieh *et al.*, 2014; Gyawali *et al.*, 2019). In 2016, 2017 and 2018, the subpopulations were grown in Columbia, Missouri, USA (Gyawali *et al.*, 2019). In 2020 the subpopulations were grown in Göttingen, Germany. In Missouri, each field had an approximate size of 0.1 ha (Gyawali *et al.*, 2019). The row-spacing was 91 cm and the space between the plants was 15 cm (Gyawali *et al.*, 2019). In Göttingen, the field size for three of the fields was 0.25 ha. One field was only 0.125 ha due to fewer seeds caused by a lower-than-expected harvest from one of the subpopulations in 2018. The distance between the seeds in Göttingen was approximately 33.3 cm and the row-spacing was approximately 1 m. The fields in Goettingen experienced noteworthy but non-devastating crow damage.

Plant height measurements were taken after flowering, from the ground up to the ligule of the flag leaf. Phenotypic data was analyzed using R version 4.0.3 (R Core Team, 2021). For phenotypic data analysis, data from 2016, 2017, 2018 and 2020 was used. The realized heritability from the breeder's equation (h^2_{bs}) was calculated as $h^2_{bs} = \frac{R}{S}$ (Lush, 1937), where S is the selection differential and R is the response to selection. The selection differential was calculated as the difference between the mean of the population and the mean of the selected portion (Lush, 1937). The response to selection was calculated as difference between the mean

154 of the previous generation and the mean of the next generation (Lush, 1937). This was done
155 between all subsequent generations.
156
157 Flowering time was measured because in maize it tends to be correlated with plant height
158 (Peiffer *et al.*, 2014; Mazaheri *et al.,* 2019). This could lead to indirect selection for flowering
159 time, thereby effecting the ability of plants to mate randomly. The possibility of this impacting
160 the effective population size is addressed below.
161
162 **Genotyping, quality control and filtering**
163 In 2020, the 96 randomly chosen plants from each subpopulation in generation four (384
164 individual plants in total) were genotyped using a genotyping-by-sequencing (GBS) approach.
165 Leaf tissue from those 384 plants was freeze-dried and shipped to the University of Wisconsin
166 Biotechnology center, Madison, WI, USA for DNA extraction, library preparation, and
167 sequencing via one lane on a NovaSeq6000 machine. Each subpopulation was sequenced on its
168 own sequencing run. Total sequencing yield from each run ranged from 125,000,000 to
169 300,000,000 fragments. Fragments had read lengths between 73 and 151 base pairs. GBS was
170 conducted using paired-end sequencing with the restriction enzyme *Ape*KI (Elshire *et al.*, 2011).
171 For SNP variant calling the GB-eaSy pipeline was used (Wickland *et al.*, 2017, Tange, 2011).
172 Reads were aligned to the 5th version of the B73 reference genome (Maize GDB, 2024) with the
173 Burrows Wheeler Aligner (Li, 2013). In total, 15,390,958 SNPs were called by the GB-eaSy
174 pipeline (Wickland *et al.*, 2017). In the GB-eaSy pipeline, the SNPs were filtered for a minimum
175 mapping and base quality of 30 with the BCFtools software (Danecek *et al.*, 2021). After filtering,

176 8,302,778 SNPs were kept. The mapping quality ranged from 30 to 60, and was on average
177 57.44. The raw read depth ranged from 161 to 4,999, and was on average 1,705 reads. The
178 average distance between adjacent markers was 257.67 bp.
179
180 Subsequent SNP filtering was conducted in R version 4.0.3 (R Core Team, 2021). Six individual
181 samples with a marker coverage below 0.1 were removed from the analysis. The 10% quantile
182 of marker coverage 0.6042, and 90% quantile was 0.7014 (supplementary figure S1). Markers
183 with an average sample read depth below 1 or above 10 were removed. This filtering threshold
184 was determined based on the distribution of read depth across all samples and markers
185 (supplementary figure S2). Furthermore, we required that every SNP marker was observed at
186 least 40 times in each subpopulation. Monomorphic and multi-allelic (>2) markers were
187 removed from the data set. The final data set contained 4,029,092 SNP markers, which were
188 used for the downstream analysis.
189
190 **Allele frequency estimation**
191 The allele frequency at each SNP was calculated in R according to its maximum-likelihood
192 estimate, which is computed by dividing the number of observations of a particular allele by the
193 number of observations in total (Beissinger *et al.*, 2014). The script is available at
194 (https://github.com/milaleonie/ExpEvo_with_replicated_selection).
195
196 **Estimating effective population size**

Effective population size was calculated using the known demographic parameters of the populations and based off the formula, $N_e = \frac{4 * N_m * N_f}{N_m + N_f}$, where N_m is the number of male and N_f the number of female individuals (Crow and Kimura, 1970). In every generation the ~5% shortest or tallest plants were harvested, amounting to ~250 plants. Under the assumption of complete random mating, all 5,000 plants could contribute as male parents for the next generation. In field trials, the assumption of random mating of all 5,000 plants is violated because of the effects of assortative mating (Allard, 1999). The number of male parents contributing to the next generation is reduced due to varying flowering dates and limited spatial pollen dispersion (Allard, 1999). Therefore, we evaluated the flowering dates of the 96 randomly chosen plants from each subpopulation to approximate the number of maximal simultaneously flowering tassels and silks in the entire population. We looked for the quantile in which the majority of silks is mature and receptive, because it was assumed that silks remain receptive up to five days after silk emergence (Nieh *et al.*, 2014). We calculated the number of flowering tassels during this time interval and projected it onto the entire subpopulation. This procedure is explained in more detail in supplementary figure S3.

Calculation of linkage disequilibrium (LD) decay

The extent of linkage disequilibrium (LD) was estimated based on 100,000 SNP markers with TASSEL v5 using the squared correlation between markers, r^2, over a window size of 2,000 bp (Bradbury *et al.*, 2007). We filtered the individuals out with a marker coverage below 0.6. For this analysis, we required that every SNP marker was observed at least 80 times in each subpopulation. This filtering resulted in 1,243,604 SNP markers. Additionally, we thinned the

219 data set by randomly sampling 10,000 markers per chromosome. LD decay was modeled with a
220 nonlinear regression model as expected value r^2 under drift-recombination equilibrium as
221 $E(r^2) = \frac{1}{(1+C)}$ and $C = 4Nc$ with N as the number of individuals at each site and C as the
222 recombination coefficient between sites (Remington *et al.*, 2001). We also created a pairwise LD
223 heatmap with the R package LDheatmap for the regions which were putatively under selection
224 (Shin *et al.*, 2006).
225
226 **Scan for selection signatures**
227
228 **Calculation of *F_{ST}Sum***
229 Our scan for selection was based on a statistic derived from F_{ST}, which we call *F_{ST}Sum*. First, F_{ST}
230 was calculated according to $F_{ST} = \frac{s^2}{\mu(p)*\mu(1-p)+\frac{s^2}{r}}$, where s^2 is the sample variance of the allele
231 frequency between populations, $\mu(p)$ is the mean allele frequency between the subpopulations
232 and r is the number of populations (Weir and Cockerham, 1984). The F_{ST} statistic was calculated
233 between the divergently selected subpopulations (Short 1 vs Tall 1; Short 2 vs Tall 2).
234 Additionally, the F_{ST} statistic was calculated between the subpopulations selected in the same
235 direction (Short 1 vs Short 2; Tall 1 vs Tall 2). Next, the sum of F_{ST} was calculated between the
236 two non-redundant comparisons of divergently selected subpopulations (Short 1 vs Tall 1; Short
237 2 vs Tall 2) and subpopulation selected in the same direction (Short 1 vs Short 2; Tall 1 vs Tall 2).
238 Assessing divergence among replicates can help in the distinction between putatively selected
239 loci and false positives (Otte and Schlötterer, 2020; Chen, Pelizzola and Futschik, 2023).
240

241 **Window-based analysis**

242 We implemented a window-based analysis to assess linked selection. A cubic smoothing spline
243 was applied to the single-marker based $F_{ST}Sum$ values. From the fitted spline, inflection points
244 were calculated and used as window boundaries for newly defined regions. This analysis was
245 performed with the R package GenWin (Beissinger *et al.*, 2015). Briefly, the GenWin package
246 returns window boundaries, which we used to define regions with linked markers that may be
247 analyzed together (Beissinger *et al.*, 2015). However, the windows are of variable sizes, so we
248 used the W statistic (*Wstat*), as defined by Beissinger *et al.* (2015), to correct for this. *Wstat* is
249 defined according to $Wstat = \frac{(X-\mu)}{\sqrt{\frac{s^2}{n}}}$, where X is the mean $F_{ST}Sum$ of a window, μ is the mean
250 $F_{ST}Sum$ of the entire data set, s^2 is the sample variance of $F_{ST}Sum$ values across the entire data
251 set and n is the number of markers. *Wstat* can therefore be used to compare regions, despite
252 each consisting of a different number of markers (Beissinger *et al.*, 2015).

253

254 **Calculation of significance thresholds**

255 Significance thresholds for selection were calculated in two ways: 1) based on the empirical
256 distribution (as a baseline to compare to); and 2) based on the FDRfS (Turner and Miller, 2012).

257 1) The significance thresholds based on the empirical distribution were calculated by taking
258 the 99.9th and the 99.99th percentile of the entire distribution of the *WStat* values (Akey,
259 2009; Beissinger *et al.*, 2014; Hirsch *et al.*, 2014; Ma *et al.*, 2015; Cesconeto *et al.*, 2017;
260 Wang *et al.*, 2018; Ayalew *et al.*, 2020).
261 2) High *Wstat* values based on $F_{ST}Sum$ values calculated between divergently selected
262 subpopulations are observed when the sites located in the region showed the same

263 pattern of differentiation in both comparisons. Regions with high *Wstat* based on F_{ST}*Sum*
264 values calculated between subpopulations selected in the same direction are false
265 positive observations for selection for plant height. By dividing the number of regions
266 diverged between the subpopulations selected in the same direction by the number of
267 regions diverged between the divergently selected subpopulation for each observation
268 of *Wstat*, we obtained the false discovery rate for selection (FDRfS) for *Wstat*. The FDRfS
269 was calculated for all observed windows (Turner and Miller, 2012). We identified the
270 maximum *Wstat* value observed from comparisons between the subpopulations
271 selected in the same direction, and used this as our significance threshold.
272 To visualize the scope of selection and drift, Turner and Miller (2012) plotted the allele
273 frequency differences from the comparisons of divergently selected subpopulations and
274 subpopulation selected in the same direction against each other. This plot is referred as the
275 "Sauron plot". We created this plot with F_{ST}, which resulted in a "Quarter-Sauron" plot, because
276 F_{ST} ranges from 0 to 1, whereas allele frequency differences range from -1 to 1. Both plots are
277 available in supplemental file S4. These plots depict how the FDRfS is computed and provides a
278 visualization of the scope of drift and selection.
279
280 **Haplotype estimation and haplotype block calculation**
281 The data was phased using fastPHASE version 1.4.8 (Sheet and Stephens, 2006). We phased the
282 genomic data of the regions significantly under selection with 10 iterations of the expectation-
283 maximization (EM) algorithm (Sheet and Stephens, 2006). The phased haplotypes were used for
284 plotting and the construction of the LD heatmap. Additionally, we phased 39 random regions

285 across the entire genome, with the same physical length and marker density like the region
286 significantly under selection from 9.411 to 10.423 Mb on chromosome 3. On all these regions
287 we estimated haplotype blocks with the R package HaploBlocker (Pook *et al.*, 2019). In the
288 HaploBlocker package, a haplotype block is as a sequence of genetic markers of arbitrary length
289 with a particular frequency in the population (Pook *et al.*, 2019). The haplotype blocks only
290 contain haplotypes with a similar sequence of markers (Pook *et al.*, 2019). This helps to simplify
291 the common haplotypes. The average number of haplotype blocks, the average block length and
292 the total block number was calculated for all regions in the different subpopulations.
293

294 ## Results

295 **Phenotypic evaluation**

296 We observed notable and significant plant height differences between the subpopulations
297 selected in opposite directions (Figure 2). After three generations of selection, the mean plant
298 height difference between subpopulations selected in the opposite direction was 66.55 cm (P ~
299 0). The mean plant height decreased in the subpopulations selected for short plant height by
300 22.92 cm (P ~ 0) and increased in the subpopulations selected for tall plant height by 30.61 cm
301 (P ~ 0). Throughout the experiment, the response to selection was always negative in the
302 subpopulations selected for short plants and always positive in the subpopulations selected for
303 tall plants (Figure 2).
304

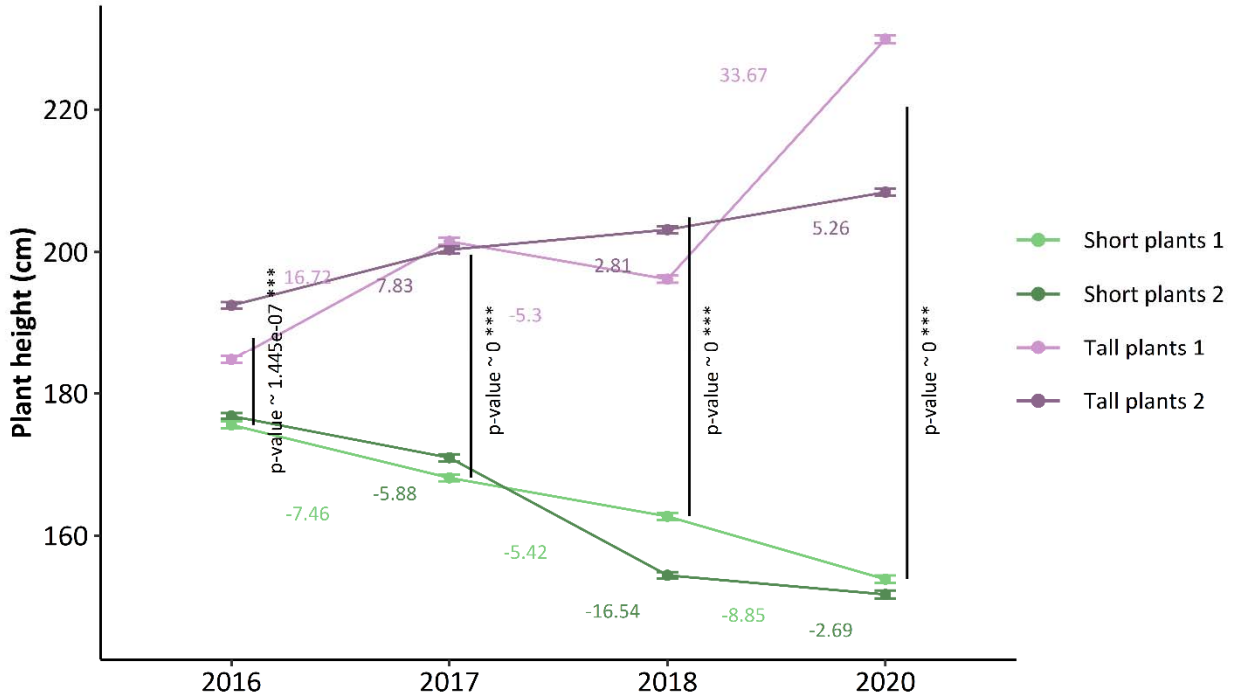

Figure 2: Mean plant height in each generation of selection. Error bars indicate a confidence interval for our estimation of means.

Realized heritability was computed by using the breeder's equation (h^2_{bs}) (Lush, 1937), and was estimated to be 0.3. Since each population was evaluated in a different environment (i.e. the year and location where it was selected), this application of the breeder's equation should be considered only approximate. Plant height and flowering time were correlated in the subpopulations short 1, short 2, tall 1, and tall 2 with correlation coefficients of 0.2183 (P ~ 0.0376), -0.0384 (P ~ 0.7165), 0.2709 (P ~ 0.0107) and 0.4572 (P ~ 0), respectively.

Effective population size and inbreeding

The effective population size under the assumption of complete random mating was 952 individuals. Due to differences in flowering time between plants, the assumption of random mating is violated. Based on observed flowering times, we estimated that ~ 59.38% and ~

320 82.29% in the short and ~ 56.25% and ~ 38.54% in the tall subpopulations had the potential to
321 pollinate one another. When we re-estimated effective population size based on this number of
322 male plants, the effective population size was estimated ~ 922 and ~ 943 individuals in the short
323 subpopulations and ~ 918 and ~ 885 individuals in the tall subpopulations.
324
325 **Comparison of significance thresholds and candidate gene identification**
326 As a baseline for comparison, we also evaluated using outlier-based significance thresholds.
327 Thresholds based on the 99.9th and the 99.99th percentile of the empirical distribution were
328 exceeded, respectively, by 93 and 10 different regions (Figure 3A). Significance thresholds based
329 on the FDRfS were exceeded by three different regions (Figure 3A). This demonstrates that had
330 we utilized outlier-based significance thresholds in this experiment, we would have identified
331 several false positive candidates for selection. *Wstat* values calculated between the
332 subpopulations selected in the same direction are depicted in Figure 3B.

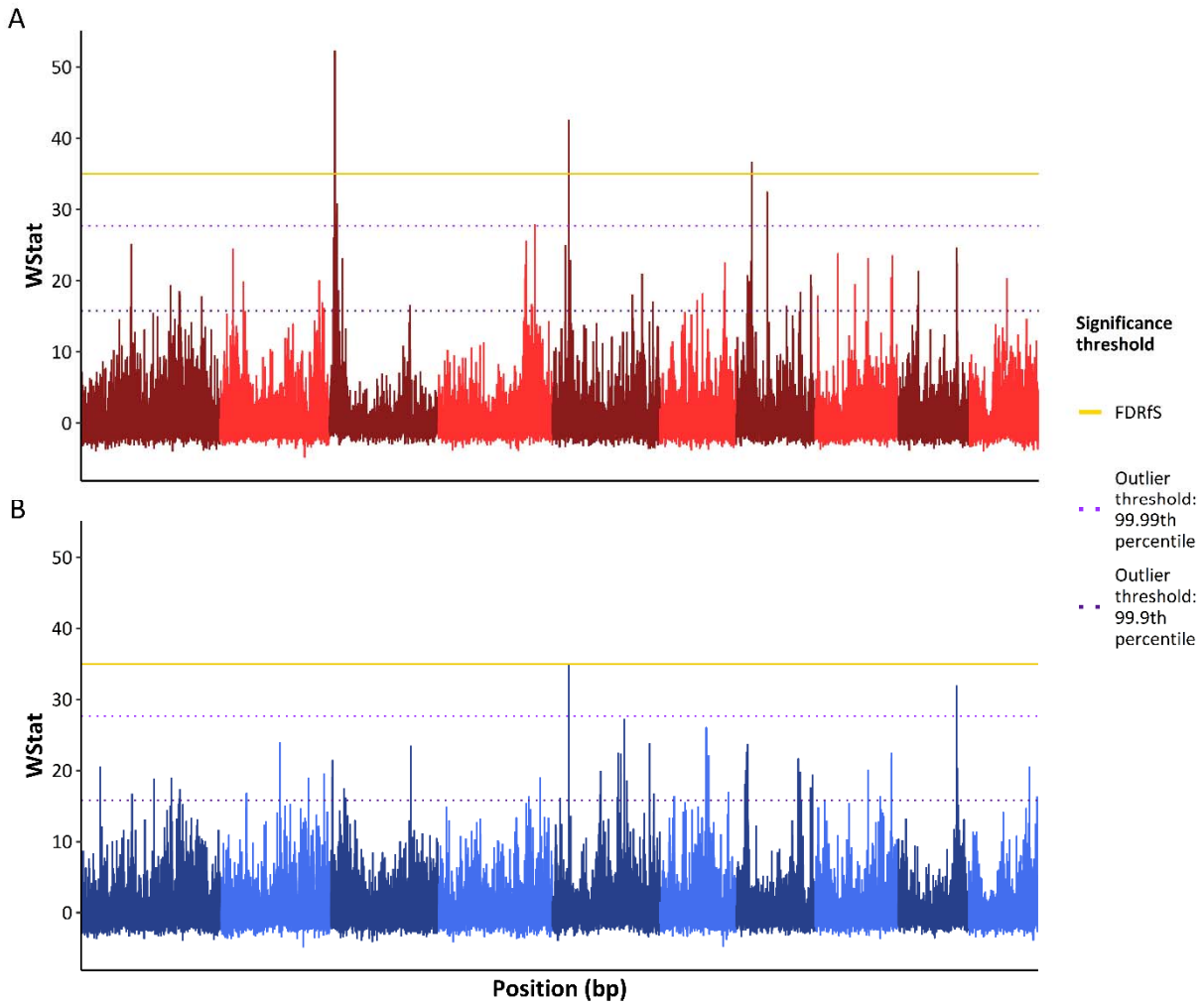

Figure 3: Differentiation along the entire genome expressed by *Wstat* calculated based on F_{ST} at each SNP marker between the subpopulations selected in opposite directions (A) and the same direction (B) with the significance thresholds based on the 99.9th percentile of the empirical distribution (light purple), based on the 99.99th percentile of the empirical distribution (dark purple), and by the false discovery rate for selection (FDRfS) (yellow).

In supplemental S8, we included the results from $F_{ST}Sum$ values observed at single SNP markers plotted against their positions.

Candidate plant height SNPs

All three regions under selection identified based on *Wstat* overlapped with coding regions in the B73 v5 annotated gene models (Maize GDB, 2024). The region with the highest *Wstat* value

345 was located on chromosome 3 from 9.911 to 9.923 Mb (Figure 4). This 12 kb region is ~ 138 kb
346 away from *iAA8,* and is ~ 518 kb away from *Dwarf 1* (Figure 4). The region is also 31 kb away
347 from a significant marker identified in the Gyawali *et al.* (2019) study (Figure 4). The region was
348 close to the coding region of other annotated gene models like *defective kernel5*, *glossy13* and
349 *bzr6* (BZR-transcription factor 6) (Figure 4), but for these no previous evidence for their impact
350 on plant height was found based on a literature review. We also observed other gene models,
351 shown as yellow arrows, which are included in supplemental S10.
352

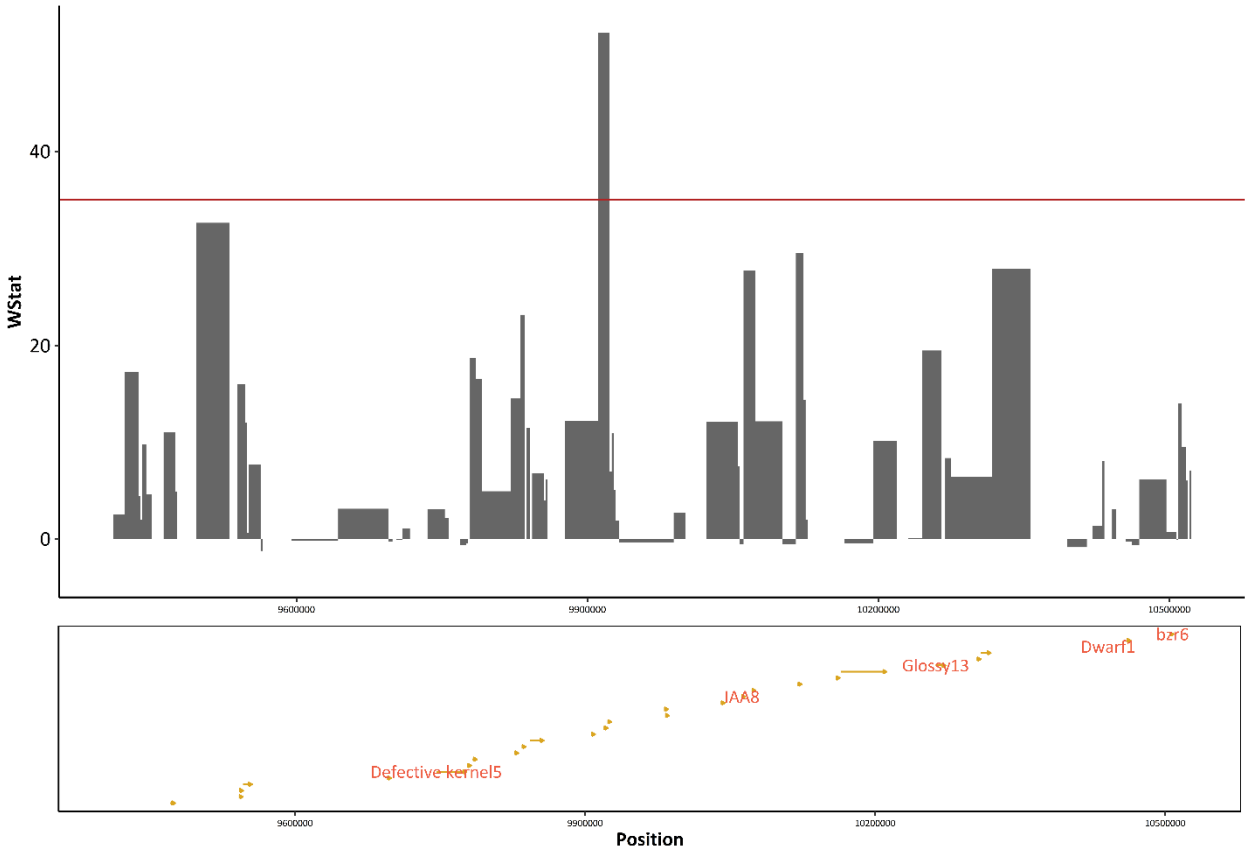

353
354 **Figure 4:** Putatively selected region on chromosome 3 from 9.911 to 9.923 Mb and 0.5 Mb up- and downstream
355 and the coding regions of the gene models in this region.
356

357 The plant height genes *Dwarf1* and the *iAA8* have already been shown to be directly involved in
358 plant height differences in many studies (Teng *et al.*, 2013; Peiffer *et al.*, 2014; Liu, Fernie and
359 Yan, 2020; Ramos Báez *et al.*, 2020). Therefore, these genes related to plant height were used as
360 ground truth to test the method. Other neighboring gene models did not show a known
361 connection to plant height based on a review of the literature.
362
363 The region on chromosome 5 from 30.103 to 30.115 Mb also had a length of 12 kb. This region
364 was 32.39 kb downstream from the coding region of the gene *importin beta24* (Figure 5). The
365 gene *importin beta24* is responsible for the mediation of the nucleocytoplasmic transport (Jin *et*
366 *al*., 2022), and there is a study which reports a connection to dwarfism in Arabidopsis (Panda *et*
367 *al*., 2020). However, a literature review revealed no evidence of its direct effects on plant height
368 in maize. We also observed other gene models, shown as yellow arrows, which are included in
369 supplemental S10.

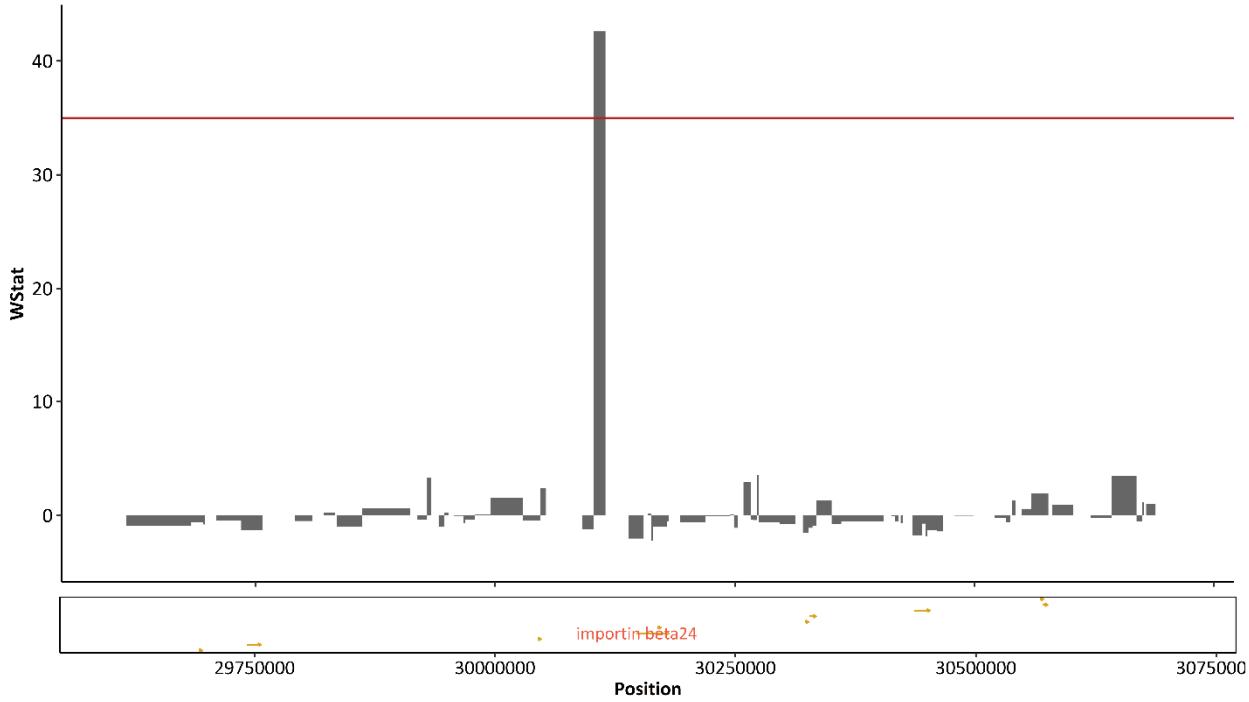

Figure 5: Putatively selected region on chromosome 5 from 30.103 to 30.115 Mb and 0.5 Mb upstream and downstream and the coding regions of the gene models in this region.

The region on chromosome 7 from 42.687 to 42.725 Mb had a length of 38 kb and was 435 kb upstream from the coding region of the gene model *beta expansin4* also referred as *expb4* (Figure 6). The gene *beta expansin4* is responsible for expansin protein which are capable of inducing cell wall extension in maize (Wu *et al.*, 2001). But also, for this gene model no further evidence for their impact on plant height in maize was found based on a literature review. We also observed other gene models, shown as yellow arrows, which are included in supplemental S10.

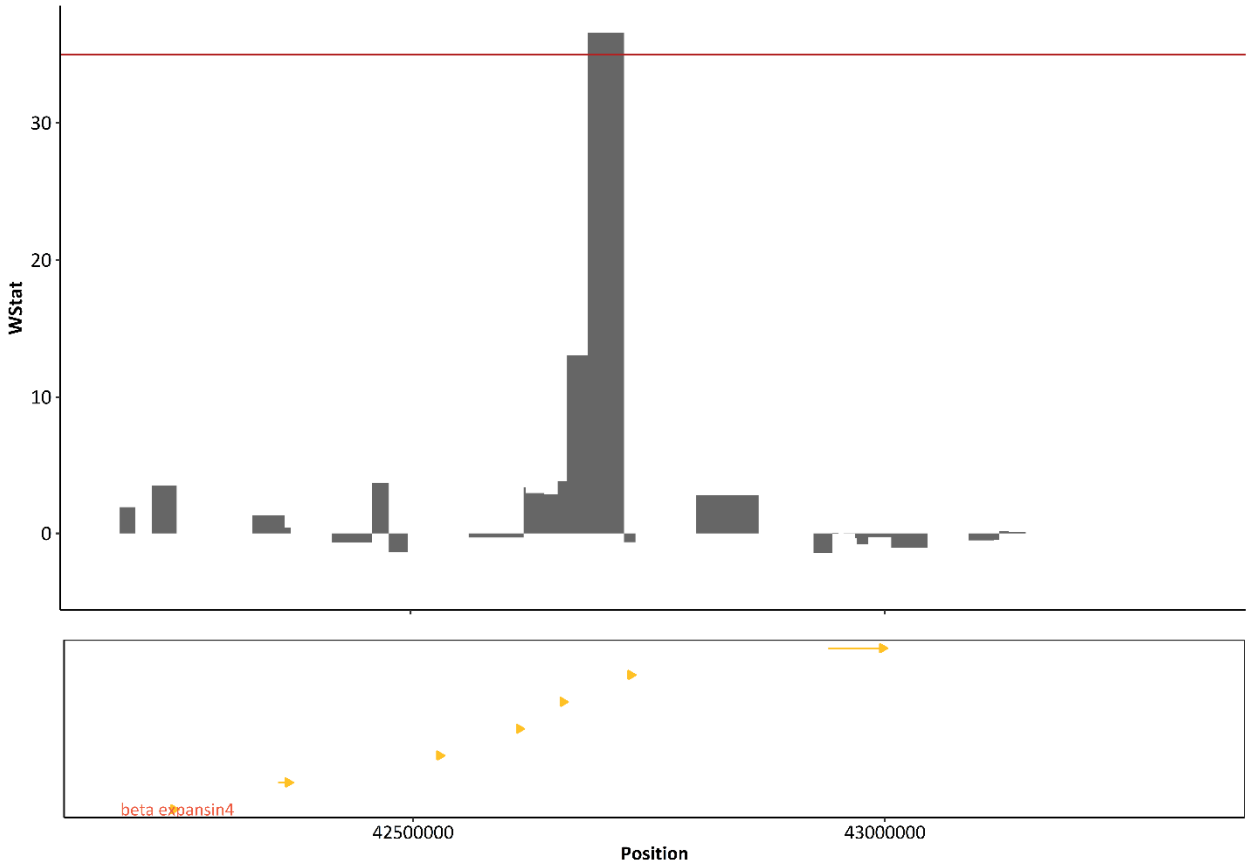

Figure 6: Putatively selected region on chromosome 7 from 42.687 to 42.725 Mb and 0.5 Mb up- and downstream and the coding regions of the gene models in this region.

Haplotype block analysis

We investigated the regions putatively under selection in more detail by dissecting the haplotypes in the subpopulations. The haplotypes from the region from 9.911 to 9.923 Mb and 0.5 Mb up- and downstream on chromosome 3 are shown in Figure 7A. We observe different haplotypes across the entire region (Figure 7A). From ~10.4131 to ~10.4132 Mb, only 27.79 kb from the coding region of *Dwarf1*, we observed different alleles in the divergently selected subpopulations (Figure 7A). Also, from 10.0539 to 10.0646 Mb, located within the coding region of *iAA8*, a similar pattern of divergence is observed between the divergently selected subpopulations (Figure 7A). We also observed variation in haplotypes from 9.42 to 9.448 Mb

395 and from 9.4712 to 9.563 Mb (Figure 7A). To supplement our haplotype investigation, we
396 looked at LD across putatively selected regions in the different subpopulations. The pairwise LD
397 heatmap indicates strong LD across the entire region from 9.911 to 9.923 Mb and 0.5 Mb up-
398 and downstream in the subpopulations selected for short plant height (Figure 7B). We observed
399 a low LD across the entire region in the subpopulations selected for tall plant height (Figure 7B).
400

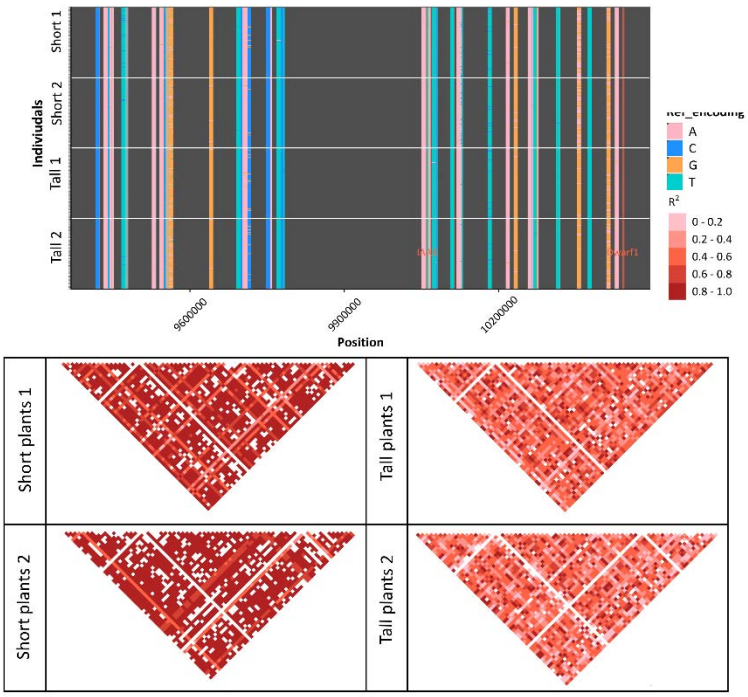

401
402 **Figure 7:** Putatively selected region on chromosome 3 from 9.911 to 9.923 Mb and 0.5 Mb up- and downstream
403 and the observed haplotypes (A) and pairwise LD heatmap for the different subpopulations (B).
404

405 The haplotypes in the region from 30.103 to 30.115 Mb and the neighboring area of 0.5 Mb
406 upstream and downstream on chromosome 5 are shown in Figure 8A. We observe large
407 variation in the haplotypes around ~ 29.8079, ~ 29.8303, ~ 30.2666 and ~30.3253 Mb (Figure
408 9A). The pairwise LD heatmap indicates strong LD across the entire region in all subpopulations
409 with no differences between the different subpopulations (Figure 8B).
410

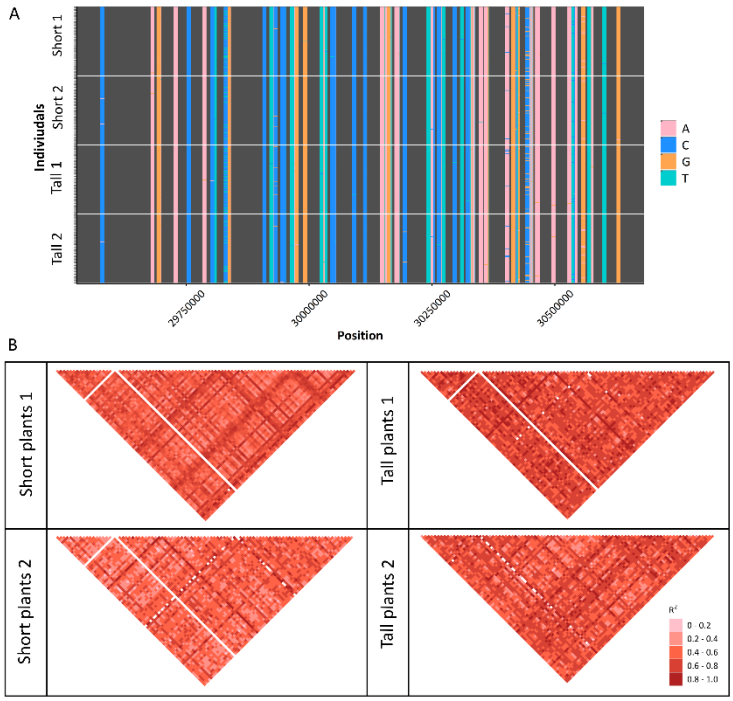

Figure 8: Putatively selected region on chromosome 5 from 30.103 to 30.115 Mb and 0.5 Mb upstream and downstream and the observed haplotypes (A) and pairwise LD heatmap for the different subpopulations (B).

Figure 9A shows the haplotypes in the region on chromosome 7 from from 42.687 to 42.725 Mb and 0.5 Mb up- and downstream. We observe large variation in the haplotypes around ~ 42.6 Mb in many small regions (Figure 9A). We also observe variation around 42.2 Mb and from 42.432 to 42.49 Mb (Figure 9A). The pairwise LD heatmap indicates varying LD across the entire region in all subpopulations (Figure 8B). But overall, we observed a lower LD across the entire region in the subpopulations selected for short plant height and a stronger LD in the subpopulations selected for tall plant height (Figure 7B).

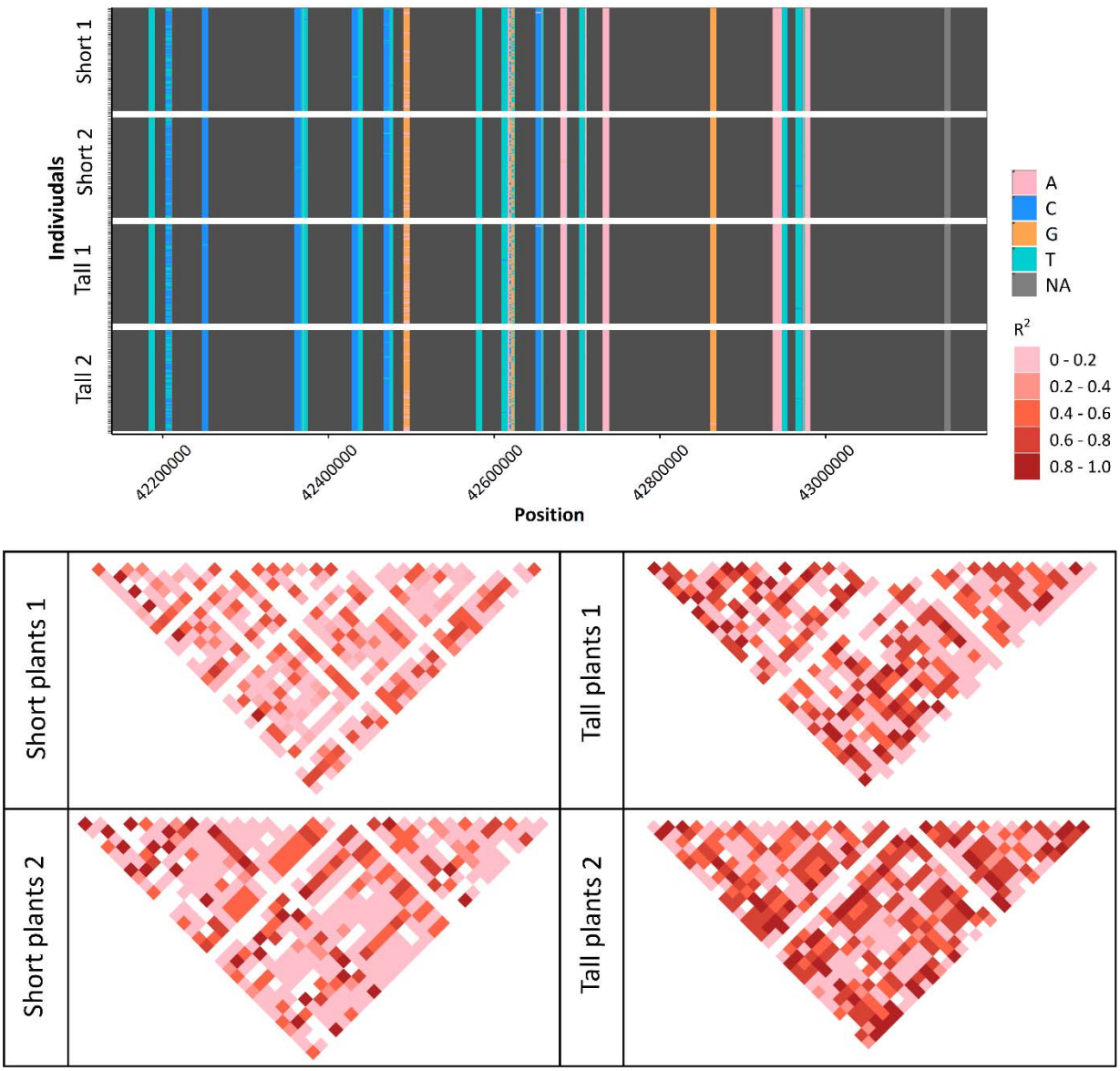

Figure 9: Putatively selected region on chromosome 7 from from 42.687 to 42.725 Mb and 0.5 Mb up- and downstream and the observed haplotypes (A) and pairwise LD heatmap for the different subpopulations (B).

Discussion

In contrast to most agriculture long-term selection experiments, our study included replication of the evolutionary process. This allowed us to directly compare the commonly used approaches to significance threshold specification leveraging replications. Our results demonstrate that

432 significance thresholds specified using evolutionary replicates can widely vary from thresholds
433 based on empirical outliers. Because linkage leads to selection operating on regions instead of
434 individual markers, we used the R package GenWin (Beissinger *et al.*, 2015) to calculate *Wstat*
435 values based on a cubic smoothing spline applied to $F_{ST}Sum$.
436
437 Significance thresholds based on the FDRfS identified fewer markers than outlier-based
438 significance thresholds. Because these thresholds are based on replication, markers exceeding
439 them are expected to correspond to true signals of selection. Previous studies applied
440 significance thresholds based on the FDRfS on statistics like Chi-Square (Linder *et al.*, 2021) and
441 allele frequency differences (Turner and Miller, 2012). We adapted the calculation of the FDRfS
442 to $F_{ST}Sum$, a version of F_{ST} which leverages replications. For comparison, we also explored
443 calculating FDRfS from allele frequency differences (DiffStat) as was done by Turner and Miller
444 (2012). The results are available in supplementary figures S4, S5 and S7. We identified more
445 significant markers using the FDRfS from $F_{ST}Sum$ approach in comparison to allele frequency
446 differences (DiffStat). This was also observed by Kofler and Schlötterer (2014). Our window-
447 based approach seems to be the more suitable method than single marker based $F_{ST}Sum$ values
448 since the single marker based $F_{ST}Sum$ would have returned many single markers tagging the
449 same region as it is shown in supplemental file S9.
450
451 The region on chromosome 3 from 9.911 to 9.923 Mb was very close to a marker from previous
452 study by Gyawali *et al.* (2019). Furthermore, the gene models *iAA8, Dwarf1*, *defective kernel5*,
453 *glossy13* and *bzr6* were found close to this region. The plant height genes *iAA8* and *Dwarf1* are~

454 138 kb and ~ 518 kb away from the putatively selected region from 9.911 to 9.923 Mb on
455 chromosome 3.
456
457 *Dwarf1* is involved in the expression of gibberellin 3-oxidase (Teng *et al.*, 2013). High expression
458 of the gene leads to high levels of bioactive gibberellin and results in taller plants (Teng *et al.*,
459 2013). When the *Dwarf1* gene is not expressed, plants exhibit the *Dwarf1* phenotype, which is
460 characterized by dwarfism (Teng *et al.*, 2013). Multiple gene expression studies have previously
461 reported that this gene has a large effect on plant height (Teng *et al.*, 2013; Liu, Fernie and Yan,
462 2020). In one experiment, this gene explained 32.3% of the phenotypic variance for plant height
463 (Teng *et al.*, 2013). The *iAA8* gene regulates auxin biosynthesis, transport, and signaling
464 (Matthes *et al.*, 2019; Ramos Báez *et al.*, 2020). Auxin is a plant hormone and plays a key role in
465 plant growth and development (Ramos Báez *et al.*, 2020). The *iAA8* gene was also observed to
466 regulate maize inflorescence architecture (Galli *et al.*, 2015; Ramos Báez *et al.*, 2020). Both
467 genes appear to be causal for plant height differences based on the literature (Teng *et al.*, 2013;
468 Peiffer *et al.*, 2014; Liu, Fernie and Yan, 2020; Ramos Báez *et al.*, 2020). Therefore, these plant
469 height genes were used as ground truth to test the method.
470
471 The *defective kernel 5* gene model was reported to cause reduced starchy endosperms and
472 leads to a shrunken or collapsed endosperm (Zhang *et al*., 2019). *Glossy13* encodes a putative
473 ABC transporter required for the accumulation of epicuticular waxes, which also help to control
474 water loss (Li *et al*., 2013). The gene model *bzr6* is a transcription factor for brassinosteroids
475 which are plant specific steroidal hormones (Manoli *et al*., 2017). Brassinosteroids contribute to

476 regulating a broad spectrum of plant growth and developmental processes in maize (Manoli *et*
477 *al*., 2017).
478
479 Very close to the coding region of *Dwarf1* and within the coding region *iAA8*, we observed
480 different haplotypes in the divergently selected subpopulations (Figure 7A). Overall, we
481 observed stronger LD in the putatively selected region on chromosome 3 in the subpopulations
482 selected for short plants. These differences may indicate stronger selection in the
483 subpopulations selected for short plants.
484
485 This could theoretically be a result of more inbreeding in the short subpopulations, which we
486 tested by evaluating haplotype blocks in 39 random regions of the genome. The random regions
487 were of equal size and marker density to the putatively selected region on chromosome 3. We
488 observe on average 31 blocks in short 1, 30 blocks in short 2, 31 blocks in tall 1 and 34 blocks in
489 tall 2. The blocks have an average block size of 402.8 bp in short 1, 427.36 bp in short 2, 409.01
490 bp in tall 1 and 404.76 bp in tall 2. This indicates that the tall subpopulations show similar levels
491 of inbreeding to the short subpopulations. Results from the calculated haplotype blocks from
492 the 39 random regions are available in supplementary figure S11 and S12.
493
494 Overall, a slow decline in LD was observed with increasing physical distance across all
495 chromosomes (Supplemental S13). R^2 of 0.1 was observed at a distance of 2 Mb (Supplemental
496 S13). But when we consider the subpopulations separately in the pairwise LD heatmap, we
497 observe very different results (Figure 7B). In the pairwise LD heatmap calculated for each

498 subpopulation and the different regions, we observed strong variation in LD between the
499 divergently selected subpopulations and between the different regions (Figure 7B).
500
501 The observation of strong LD in the putatively selected region on chromosome 3 in the short
502 plant populations supports the argument that strong selection may act on the entire candidate
503 gene region in theses populations (Franssen, Barton and Schlötterer, 2016; Barghi and
504 Schlötterer, 2019, Otte and Schlötterer, 2020; Schlötterer, 2023). The strength of selection and
505 the experimental design influence hitchhiking (Baldwin-Brown, Long and Thornton, 2014; Kofler
506 and Schlötterer, 2014). We applied a strong selective regime in our experiment in comparison to
507 previous studies (Kofler and Schlötterer, 2014; Long *et al.*, 2015). Strong selection leads to more
508 hitchhiking and a lower mapping resolution (Kofler and Schlötterer, 2014), which we observe in
509 the short subpopulations. Another reason for strong selection acting on entire regions could be
510 that many loci in this region are linked, resulting in joint selection (Schlötterer, 2023). However,
511 strong LD may also persist due to more inbreeding in the short subpopulations. But we only
512 observe strong LD in the short subpopulations in our putatively selected region on chromosome
513 3. On the other hand, we observed stronger LD in the tall subpopulations in our putatively
514 selected region on chromosome 7 and similar LD patterns among all subpopulations in our
515 putatively selected region on chromosome 5. When we calculated the pairwise LD heatmap for
516 the different subpopulations in two random regions (supplementary figures S14 and S15), we
517 did not observe a similarly strong difference in LD between the subpopulations as we did for the
518 putatively selected region on chromosome 3 (Figure 7).
519

520 Even though we observed stronger LD in the tall subpopulations across our putatively selected
521 region on chromosome 7, we also observed variation in LD. This may be because this small
522 region is under selection. We also observed large variation in the haplotypes in this region,
523 whereas most of the neighboring regions exhibit fixed haplotypes. The putatively selected
524 region is only 22.78 kb from an uncharacterized protein (see supplemental S10), whereas *beta*
525 *expansin4* is located 32.39 kb away from this region (Maize GDB, 2024). The gene *beta*
526 *expansin4* is responsible for expansin protein which are capable of inducing cell wall extension
527 in maize (Wu *et al.*, 2001).
528
529 Close and within the other putatively selected regions on chromosome 5, several gene models
530 were found but based on our literature review, no previous evidence for their impact on plant
531 height was found. The gene model *importin beta24* is located on chromosome 5 and was 32.39
532 kb upstream from the putatively selected region on this chromosome (Maize GDB, 2024). Across
533 this region and its neighboring area, we observed strong LD across all subpopulations. We
534 observed variation in haplotypes in smaller neighboring segments of the coding region of
535 *importin beta24*. This may indicate that this gene model is under selection. The gene *importin*
536 *beta24* is responsible for the mediation of the nucleocytoplasmic transport (Jin *et al.*, 2022), but
537 there is a study which reports a connection to dwarfism in Arabidopsis (Panda *et al.*, 2020).
538 These gene models and the gene model *bzr6* on chromosome 3 may be interesting candidates
539 for further studies to test their effect on plant height.
540

541 It is not only the strength of selection that can influence the number of variants selected in
542 experimental evolution studies. The number of selected variants also depends highly on
543 experimental design factors such as the population size, the duration of the experiment, the
544 applied selective regime (Kofler and Schlötterer, 2014; Kessner and Novembre, 2015; Lai *et al*.,
545 2024), and the species (Tobler *et al*., 2014; Barghi *et al.*, 2017). Divergent selection can increase
546 the power of the experiment in comparison to a single direction experiment (Kessner and
547 Novembre, 2015). We observe differences regarding the resolution between the subpopulations
548 selected in divergent directions. Even though the same strength of selection is applied in the
549 divergently selected subpopulations, differences between the subpopulations can be observed
550 (Moose, Dudley and Rocheford, 2004). But, these differences indicate that there is an increase
551 in power due to divergent selection (Kessner and Novembre, 2015; Schlötterer, 2023).
552
553 Previous simulation studies investigating experimental evolution have demonstrated that
554 replication is one of the most powerful tools to increase power (Kofler and Schlötterer, 2014;
555 Otte & Schlötterer, 2020, Phillips *et al.*, 2020). In fact, Kofler and Schlötterer (2014) observed
556 that replication is more important for detecting variants than population size (Kofler and
557 Schlötterer, 2014; Kessner and Novembre, 2015; Barghi, Hermisson and Schlötterer, 2020).
558
559
560 **Conclusion**
561 In conclusion, our research demonstrates that replicated selection is a powerful tool in
562 agricultural experimental evolution studies. We observed selection across replicates, even

563 though we only selected for three generations. Moreover, we saw that a significance threshold
564 based on the FDRfS is more reliable than existing methods for significance threshold
565 identification. The application of a cubic smoothing spline to single marker-based statistics like
566 $F_{ST}Sum$ to return window boundaries of regions which are putatively under selection helped
567 collapse signal from multiple hitchhiking markers. Haplotype block analysis additionally helped
568 to investigate the regions putatively under selection. We observe very different patterns of
569 selection in divergently selected subpopulations, which might be due to selection. After more
570 generations of selection, and a reduction of linkage between putatively selected loci and neutral
571 loci, we may draw more certain conclusions about selection for the plant height genes.
572 Furthermore, we might be able to identify significant markers close to our plant height
573 candidate genes and novel gene loci without any associated gene models.
574

575 **Availability of data and materials**

576 All the data and statistics about the present study has been included in the current manuscript
577 in the form of figure and tables. Raw data are publicly available at figshare;
578 https://figshare.com/projects/Shoepeg_ExpEvo2020/139981. Our analysis code is available
579 publicly on github: https://github.com/milaleonie/ExpEvo_with_replicated_selection.
580
581

582 **Acknowledgements**

583 Abiskar Gyawali contributed substantially to this study but passed away before submission.
584 Journal policy prohibits him from being listed as a co-author because he could not approve the

final manuscript. We consider Abi to be an important co-author of this manuscript, are grateful for his contributions, and miss him tremendously. Kate Guill was instrumental in conducting early-generation seed increase and field management in Missouri.

Funding

This work was supported by startup funds provided by the University of Goettingen. The first two generations of selection were funded by the USDA Agricultural Research Service. We utilized the computational resources of the University of Goettingen's GWDG.

Conflict of interest

The author declares that there is no conflict of interest.

References

Akey JM, G Zhang, K Zhang, L Jin, and MD Shriver. Interrogating a High-Density SNP Map for Signatures of Natural Selection. Genome Research. 2002;12(12): 1805–1814.

Akey JM. Constructing genomic maps of positive selection in humans: Where do we go from here? Genome Research. 2009;19(5): 711–722.

Allard RW. Principles of plant breeding. 2nd ed. New York: J. Wiley. 1999.

Angert AL, Bradshaw HD Jr., and Schemske DW. Using Experimental Evolution to Investigate Geographic Range Limits in Monkeyflowers. Evolution. 2008;62(10): 2660–2675.

Ayalew H, ME Sorrells, BF Carver, PS Baenziger, XF Ma. Selection signatures across seven decades of hard winter wheat breeding in the Great Plains of the United States. The Plant Genome. 2020;13(3).

Baldwin-Brown JG, A Long and KR Thornton. The power to detect quantitative trait loci using resequenced, experimentally evolved populations of diploid, sexual organisms. Molecular Biology and Evolution. 2014; 31(4): 1040-55.

Barghi N, R Tobler, V Nolte, C Schlötterer. Drosophila simulans: A Species with Improved Resolution in Evolve and Resequence Studies. G3 Genes|Genomes|Genetics. 2017; 7(7): 2337–2343.

Barghi N, R Tobler, V Nolte, AM Jakšić, F Mallard, KA Otte, M Dolezal,T Taus, R Kofler,C Schlötterer. Genetic redundancy fuels polygenic adaptation in Drosophila. PLOS Biology. 2019; 17(2): 1–31.

Barghi N, C Schlötterer. Shifting the paradigm in Evolve and Resequence studies: From analysis of single nucleotide polymorphisms to selected haplotype blocks. Molecular Ecology. 2019; 28: 521–524.

Barghi N, J Hermisson, C Schlötterer. Polygenic adaptation: a unifying framework to understand positive selection. Nature reviews. 2020; 21: 769–781.

Barrick JE, DS Yu, SH Yoon, H Jeong, TK Oh, D Schneider, RE Lenski, JF Kim. Genome evolution and adaptation in a long-term experiment with Escherichia coli. Nature. 2009; 461(7268): 1243–1247.

Beissinger TM, GJM Rosa, SM Kaeppler, D Gianola, N de Leon. Defining window-boundaries for genomic analyses using smoothing spline techniques. Genetics Selection Evolution. 2015; 47(30):1-9.

Beissinger TM, CN Hirsch, B Vaillancourt, S Deshpande, K Barry, CR Buell, SM Kaeppler, D Gianola, N de Leon. A Genome-Wide Scan for Evidence of Selection in a Maize Population Under Long-Term Artificial Selection for Ear Number. Genetics. 2014; 196(3): 829–840.

Burke MK, JP Dunham, P Shahrestani, KR Thornton, MR Rose, AD Long. Genome-wide analysis of a long-term evolution experiment with Drosophila. Nature. 2010; 467(7315): 587–590.

Burke MK, Liti G, Long AD. Standing Genetic Variation Drives Repeatable Experimental Evolution in Outcrossing Populations of Saccharomyces cerevisiae. Molecular Biology and Evolution. 2014;31(12): 3228–3239.

Bradbury PJ, ZW Zhang, DE Kroon, TM Casstevens, Y Ramdoss, ES Buckler. TASSEL: software for association mapping of complex traits in diverse samples. Bioinformatics. 2007; 23(19):2633-2635.

Cesconeto RJ, S Joost, CM McManus, SR Paiva, JA Cobuci, J Braccini. Landscape genomic approach to detect selection signatures in locally adapted Brazilian swine genetic groups. Ecology and Evolution. 2017; 7(22): 9544–9556.

Chen H, M Pelizzola, A Futschik. Haplotype based testing for a better understanding of the selective architecture. BMC Bioinformatics. 2023; 24(322):1-25.

Crow JF, M Kimura. An introduction to population genetics theory. 1970. Harper & Row Publishers.

Danecek P, JK Bonfield, J Liddle, J Marshall, V Ohan, MO Pollard, A Whitwham, T Keane, SA McCarthy, RM Davies, H Li. Twelve years of SAMtools and BCFtools. GigaScience. 2021; 10(2): giab008.

Doebley J, JD Wendel, JSC Smith, CW Stuber, MM Goodman. The origin of cornbelt maize: the isozyme evidence. Economic Botany. 1988; 42(1): 120 – 131.

Dudley JW, RJ Lambert. 100 Generations of Selection for Oil and Protein in Corn. 2003. Wiley & Sons.

Elshire RJ, JC Glaubitz, Q Sun, JA Poland, K Kawamoto, ES Buckler, SE Mitchell. A Robust, Simple Genotyping-by-Sequencing (GBS) Approach for High Diversity Species. PLoS ONE. 2011; 6(5), p. e19379.

Firman RC, F Garcia-Gonzalez, E Thyer, S Wheeler, Z Yamin, M Yuan, LW Simmons. Evolutionary change in testes tissue composition among experimental populations of house mice. Evolution. 2015; 69(3): 848–855.

Franssen SU, NH Barton, C Schlötterer. Reconstruction of Haplotype-Blocks Selected during Experimental Evolution. Molecular Biology and Evolution. 2016; 34(1): 174–184.

Galli M, Q Liua, B L. Moss, S Malcomber, W Lia, C Gainese, S Federicia, J Roshkovana, R Meeley, JL Nemhauserb, A Gallavottia. Auxin signaling modules regulate maize inflorescence architecture. Proceedings of the National Academy of Sciences. 2015; 112(43): 13372–13377.

Gyawali A, V Shrestha, KE Guill, S Flint-Garcia, TM Beissinger. Single-plant GWAS coupled with bulk segregant analysis allows rapid identification and corroboration of plant-height candidate SNPs. BMC Plant Biology. 2019; 19(1):412.

Hirsch CN, SA Flint-Garcia, TM Beissinger, SR Eichten, S Deshpande, K Barry, MD McMullen, JB Holland, ES Buckler, N Springer, CR Buell, N de Leon, SM Kaeppler. Insights into the Effects of Long-Term Artificial Selection on Seed Size in Maize. Genetics. 2014;198(1): 409–421.

Janick, J. Plant Breeding Reviews: Long-Term Selection: Maize, Volume 24, Part 1. 2010a. John Wiley & Sons, Inc.

Janick, J. (2010b) Plant Breeding Reviews, Volume 24, Part 2 Long-term Selection: Crops, Animals, and Bacteria. 2010b. John Wiley & Sons, Inc.

Jin, L, GB Zhang, GX Yang, JQ Dong. Identification of the Karyopherin Superfamily in Maize and Its Functional Cues in Plant Development. International Journal of Molecular Sciences. 2022; 23(14103): 1-24.

Kessner D, J Novembre. Power Analysis of Artificial Selection Experiments Using Efficient Whole Genome Simulation of Quantitative Traits. Genetics. Genetics, 2015; 199, 991–1005.

Kofler R, C Schlötterer. A Guide for the Design of Evolve and Resequencing Studies. Molecular Biology and Evolution. 2014;31(2): 474–483.

Krimbas CB, S Tsakas. The Genetics of Dacus oleae. V. Changes of Esterase Polymorphism in a Natural Population Following Insecticide Control-Selection or Drift? Evolution. 1971; 25(3): 454–460.

Kumar R, A Gyawali, GD Morrison, CA Saski, DJ Robertson, DD Cook, N Tharayil, RJ Schaefer, TM Beissinger, RS Sekhon. Genetic Architecture of Maize Rind Strength Revealed by the Analysis of Divergently Selected Populations. Plant and Cell Physiology. 2021; 62(7): 1199–1214.

Lai WY, V Nolte, AM Jakšić, C Schlötterer. Evolution of Phenotypic Variance Provides Insights into the Genetic Basis of Adaptation. Genome Biology and Evolution. 2024; 16(4): 1-16.

Li H. Aligning sequence reads, clone sequences and assembly contigs with BWA-MEM. 2013.

Li L, D Li, SZ Liu, XL Ma, CR Dietrich, HC Hu, GS Zhang, ZY Liu, J Zheng, GY Wang, PS Schnable. The Maize glossy13 Gene, Cloned via BSR-Seq and Seq-Walking Encodes a Putative ABC Transporter Required for the Normal Accumulation of Epicuticular Waxes. PLOS ONE 8(12): e82333.

Linder RA, B Zabanavar, A Majumder, H Chiao-Shyan Hoang, VG Delgado, R Tran, VT La, SW Leemans, AD Long. Adaptation in outbred sexual yeast is repeatable, polygenic, and favors rare haplotypes. Molecular Biology and Evolution, 2022; 39(12): 1–25.

Liu J, AR Fernie, J Yan. The Past, Present, and Future of Maize Improvement: Domestication, Genomics, and Functional Genomic Routes toward Crop Enhancement. Plant Communications. 2020;1(1),100010.

Long A, G Liti, A Luptak, O Tenaillon. Elucidating the molecular architecture of adaptation via evolve and resequence experiments. Nature Reviews Genetics. 2015; 16(10): 567–582.

Lush JL. Animal Breeding Plans. Ames, Ia., Collegiate Press. 1937.

Ma Y, X Ding, S Qanbari, S Weigend, Q Zhang, H Simianer. Properties of different selection signature statistics and a new strategy for combining them. Heredity. 2015; 115(5): 426–436.

Maize GDB. Maize genetics and genomics database. 2024. www.maizegdb.org/.

Mallard F, B Afonso, H Teotónio. Selection and the direction of phenotypic evolution. eLife. 2023; 12:e80993.

Manoli A, S Trevisan, S Quaggiotti, S Varotto. Identification and characterization of the BZR transcription factor family and its expression in response to abiotic stresses in *Zea mays* L. Plant Growth Regulation. 2018; 84: 423–436.

Matthes MS, NB Best, JM Robil, S Malcomber, A Gallavotti, P McSteen. Auxin EvoDevo: Conservation and Diversification of Genes Regulating Auxin Biosynthesis, Transport, and Signaling. Molecular Plant. 2019; 12(3): 298–320.

Mazaheri M, M Heckwolf, B Vaillancourt, JL Gage, B Burdo, S Heckwolf, K Barry, A Lipzen, C Bastos Ribeiro, TJY Kono, HF. Kaeppler, EP. Spalding, CN Hirsch, CR Buell, N de Leon, SM. Kaeppler. Genome-wide association analysis of stalk biomass and anatomical traits in maize. BMC Plant Biology. 2019; 19(45): 1–19.

Moose SP, JW Dudley, TR Rocheford. Maize selection passes the century mark: a unique resource for 21st century genomics. Trends in plant science. 2014; 9: 358–364.

Michalak P, L Kang, MF Schou, HR Garner, V Loeschcke. Genomic signatures of experimental adaptive radiation in Drosophila. Molecular Ecology. 2019; 28: 600–614.

Nieh SC, WS Lin, YH Hsu, GJ Shieh, BJ Kuo. The effect of flowering time and distance between pollen source and recipient on maize. GM Crops & Food. 2014; 5(4): 287–295.

Orozco-terwengel P, M Kapun, V Nolte, R Kofler, T Flatt, C Schlötterer. Adaptation of Drosophila to a novel laboratory environment reveals temporally heterogeneous trajectories of selected alleles. Molecular Ecology. 2012; 21: 4931-4941.

Otte, KA, C Schlötterer. Detecting selected haplotype blocks in evolve and resequence experiments. Molecular Ecology Resources. 2021; 21:93–109.

Panda C, X Li, A Wager, HY Chen, X Li. An importin-beta-like protein mediates lignin-modificationinduced dwarfism in Arabidopsis. The Plant Journal. 2020; 102: 1281–1293.

Parts L, FA Cubillos, J Warringer, K Jain, F Salinas, SJ Bumpstead, M Molin, A Zia, JT Simpson, MA Quail, A Moses, EJ Louis, R Durbin, G Liti. Revealing the genetic structure of a trait by sequencing a population under selection. Genome Research. 2011; 21(7): 1131–1138.

Payen C, AB Sunshine, GT Ong, JL Pogachar, W Zhao, MJ Dunham. High-Throughput Identification of Adaptive Mutations in Experimentally Evolved Yeast Populations. PLOS Genetics. 2016; 12(10), p. e1006339.

Peiffer JA, MC Romay, MA Gore, SA Flint-Garcia, Z Zhang, MJ Millard, CAC Gardner, MD McMullen, JB Holland, PJ Bradbury, ES Buckler. The genetic architecture of maize height. Genetics. 2014; 196(4): 1337–1356.

Palma-Vera SE, H Reyer, M Langhammer, N Reinsch, L Derezanin, J Fickel, S Qanbari, JM Weitzel, S Franzenburg, G Hemmrich-Stanisak, J Schoen. Genomic characterization of the world's longest selection experiment in mouse reveals the complexity of polygenic traits. BMC Biology. 2022; 20(52): 1-20.

Phillips MA, AD Long, ZS Greenspan, LF Greer, MK Burke, B Villeponteau, KC Matsagas, CL Rizza, LD Mueller, MR Rose. Genome-wide analysis of long-term evolutionary domestication in Drosophila melanogaster. Scientific Reports. 2016; 6: 39281.

Phillips MA, IC Kutch, AD Long, MK Burke. Increased time sampling in an evolve-and-resequence experiment with outcrossing Saccharomyces cerevisiae reveals multiple paths of adaptive change. Molecular Ecology. 2020; 29: 4898–4912.

Pook, T, M Schlather, G de los Campos, M Mayer, CC Schoen, H Simianer. HaploBlocker: Creation of Subgroup-Specific Haplotype Blocks and Libraries. Genetics. 2019; 212(4): 1045–1061.

R Core Team. R: A Language and Environment for Statistical. 2021. https://CRAN.R-project.org/package=doParallel.

Ramos Báez R, RY Buckley, H Yu, Z Chen, A Gallavotti, JL Nemhauser, BL Moss. A Synthetic Approach Allows Rapid Characterization of the Maize Nuclear Auxin Response Circuit. Plant Physiology. 2020; 182(4): 1713–1722.

Remington DL, JM Thornsberry, Y Matsuoka, LM Wilson, SR Whitt, J Doebley, S Kresovich, MM Goodman, ES Buckler. Structure of linkage disequilibrium and phenotypic associations in the maize genome. PNAS. 2001; 98(20): 11479–11484.

Remolina SC, PL Chang, J Leips, SV. Nuzhdin, KA Hughes. GENOMIC BASIS OF AGING AND LIFE-HISTORY EVOLUTION IN DROSOPHILA MELANOGASTER. Evolution, 2012; 66: 3390-3403.

Romay MC, MJ Millard, JC Glaubitz, JA Peiffer, KL Swarts, TM Casstevens, RJ Elshire, CB Acharya, SE Mitchell, SA Flint-Garcia, MD McMullen, JB Holland, ES Buckler, CA Gardner. Comprehensive genotyping of the USA national maize inbred seed bank. Genome Biology. 2013; 14(R55).

Ross AJ, AR Hallauer, M Lee. Genetic analysis of traits correlated with maize ear length. Maydica. 2006; 51: 301–313.

Tange, O. GNU Parallel - The Command-Line Power Tool. The USENIX Magazine. 2011; 42-47.

Teng F, L Zhai, R Liu, W Bai, L Wang, D Huo, Y Tao, Y Zheng, Z Zhang. ZmGA3ox2, a candidate gene for a major QTL, qPH3.1, for plant height in maize. The Plant Journal. 2013; 73(3): 405–416.

Teotónio H, MR Rose. Variation in the reversibility of evolution. Nature. 2000; 408(6811): 463–466.

Tobler R, SU Franssen, R Kofler, P Orozco-terWengel, V Nolte, Joachim Hermisson, C Schlötterer. Massive Habitat-Specific Genomic Response in D. melanogaster Populations during Experimental Evolution in Hot and Cold Environments. Molecular Biology and Evolution. 2014; 31(2): 364–375.

Turner TL, AD Stewart, AT Fields, WR Rice, AM Tarone. Population-Based Resequencing of Experimentally Evolved Populations Reveals the Genetic Basis of Body Size Variation in Drosophila melanogaster. PLoS Genetics. 2011; 7(3): e1001336.

Turner TL, Miller PM. Investigating Natural Variation in Drosophila Courtship Song by the Evolve and Resequence Approach. Genetics. 2012; 191(2): 633–642.

Tusuubira SK, JK Kelly. Experimental evolution suggests rapid assembly of the 'selfing syndrome' from standing variation in *Mimulus guttatus.*Frontiers in Plant Science. 2024; 5: 1-11.

Scheet P, M Stephens. A fast and flexible statistical model for large-scale population genotype data: applications to inferring missing genotypes and haplotypic phase. American Journal of Human Genetics. 2006; 78(4): 629-644.

Schlötterer, C. How predictable is adaptation from standing genetic variation? Experimental evolution in Drosophila highlights the central role of redundancy and linkage disequilibrium. Philosphical Transactions of the Roayl Society B. 2023; 378(1877): 1-8.

Semagn, K, M Iqbal, N Alachiotis, A N'Diaye, C Pozniak, D Spaner. Genetic diversity and selective sweeps in historical and modern Canadian spring wheat cultivars using the 90K SNP array. Scientific Reports. 2021; 11 (23773): 1-16.

Silverman BW. Some Aspects of the Spline Smoothing Approach to Non-Parametric Regression Curve Fitting. Journal of the Royal Statistical Society. 1985; 47(1): 1-52

Shin J, S Blay, B McNeney, J Graham. "LDheatmap: An R Function for Graphical Display of Pairwise Linkage Disequilibria Between Single Nucleotide Polymorphisms." Journal of Statistical Software. 2006; 16(3).

U.S. National Plant Germplasm System. Details for: PI 269743, Zea mays L. subsp. mays, Shoepeg. 2021. https://www.ars-grin.gov/.

Wang K, P Wu, Q Yang, D Chen, J Zhou, A Jiang, J Ma, Q Tang, W Xiao, Y Jiang, L Zhu, X Li and G Tang. Detection of Selection Signatures in Chinese Landrace and Yorkshire Pigs Based on Genotyping-by-Sequencing Data. Frontiers in Genetics. 2018; 9:119.

Weir BS and CC Cockerham. Estimating F-Statistics for the Analysis of Population Structure. Evolution. 1984; 38(6): 1358– 1370.

Wickland DP, G Battu, KA Hudson, BW Diers, ME Hudson. A comparison of genotyping-by-sequencing analysis methods on low-coverage crop datasets shows advantages of a new workflow, GB-eaSy. BMC Bioinformatics. 2017; 18:586.

Wu YJ, ET Thorne, RE Sharp, DJ Cosgrove. Modification of Expansin Transcript Levels in the Maize Primary Root at Low Water Potentials. Plant Physiology. 2001; 126: 1471–1479.

Zhang, JY, S Wu, SK Boehlein, DR McCarty, GY Song, JW Walley, A Myers, AM Settles. Maize defective kernel5 is a bacterial TamB homologue required for chloroplast envelope biogenesis. Journal of Cell Biology. 2019; 218(8): 2638–2658.

Supplementary files

S1: Distribution of marker coverage across samples with the 10%, 35%, 65% and 90% quantiles and the cut-off at a marker coverage of 0.1 (dark red).

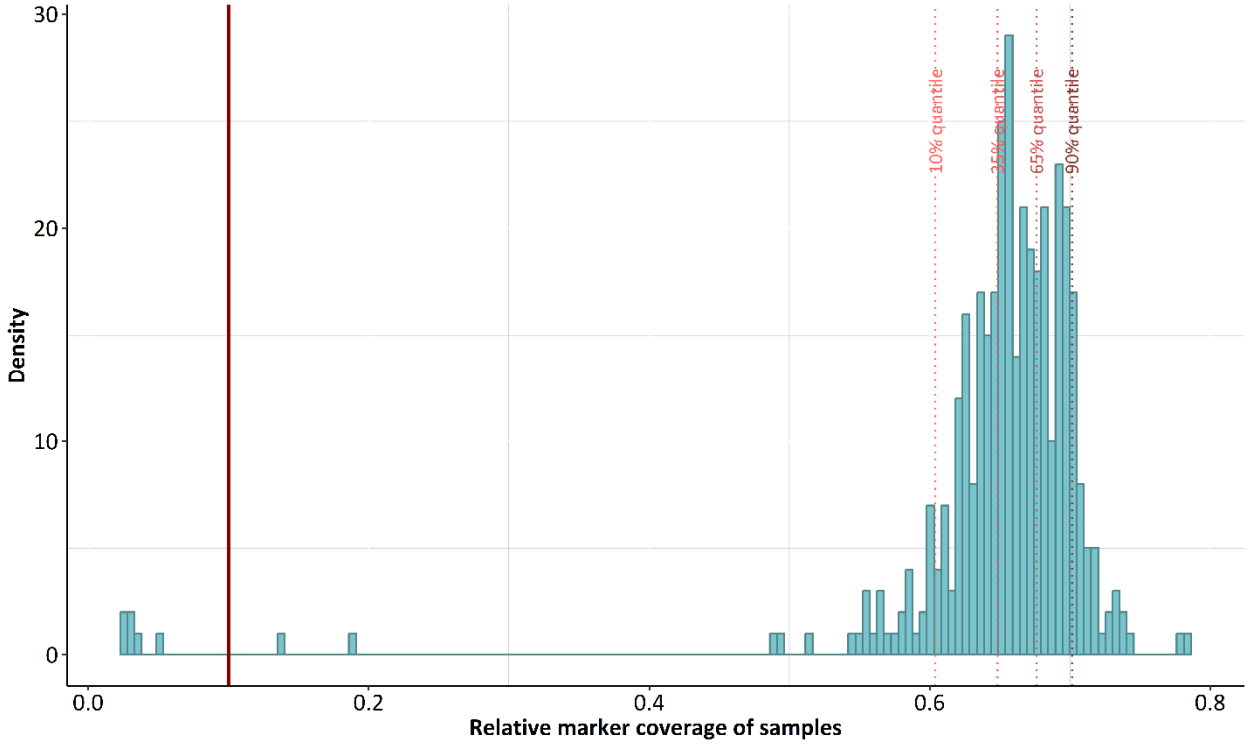

S2: Distribution of read depth across all samples and markers. Red bars represent the cutoff threshold for markers with an average sample read depth below 1 or above 10.

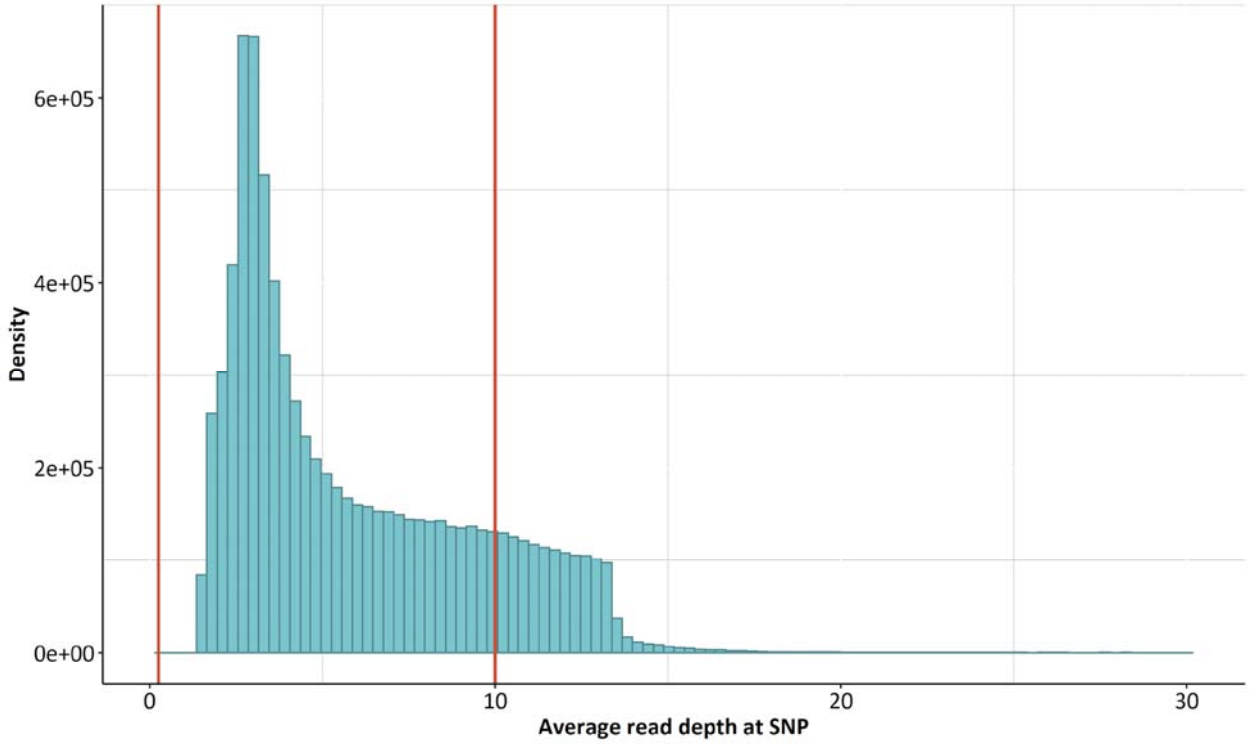

S3: Procedure for determining the number of simultaneously flowering plants and female plants in population short 1 (A), short 2 (B) and tall 1 (C) and tall 2 (D).

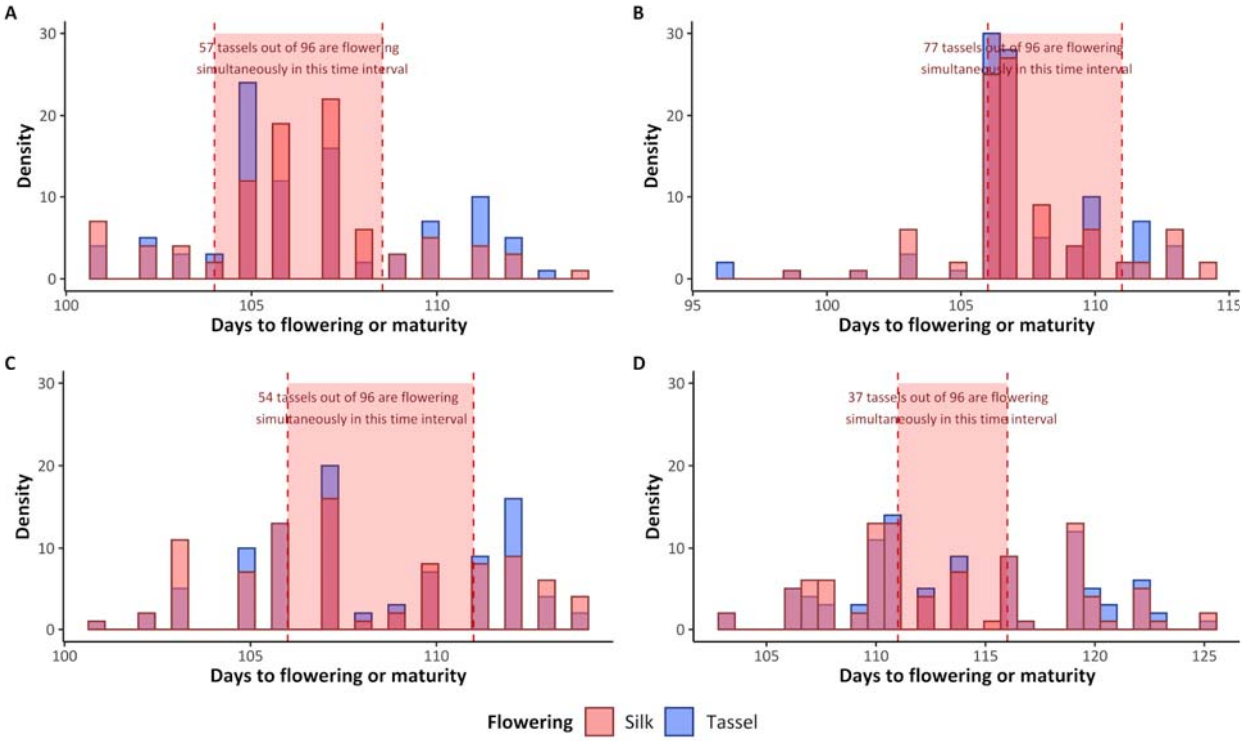

S4: "Sauron plot" for allele frequency differences (A) and "Quarter-Sauron" plot of genetic differentiation for $F_{ST}Sum$ (B) observed between the subpopulations selected in the same direction (blue) and in opposite directions (red). Each dot represents one SNP. The semi-transparent red regions correspond to a false discovery rate for selection (FDRfS) <5%.

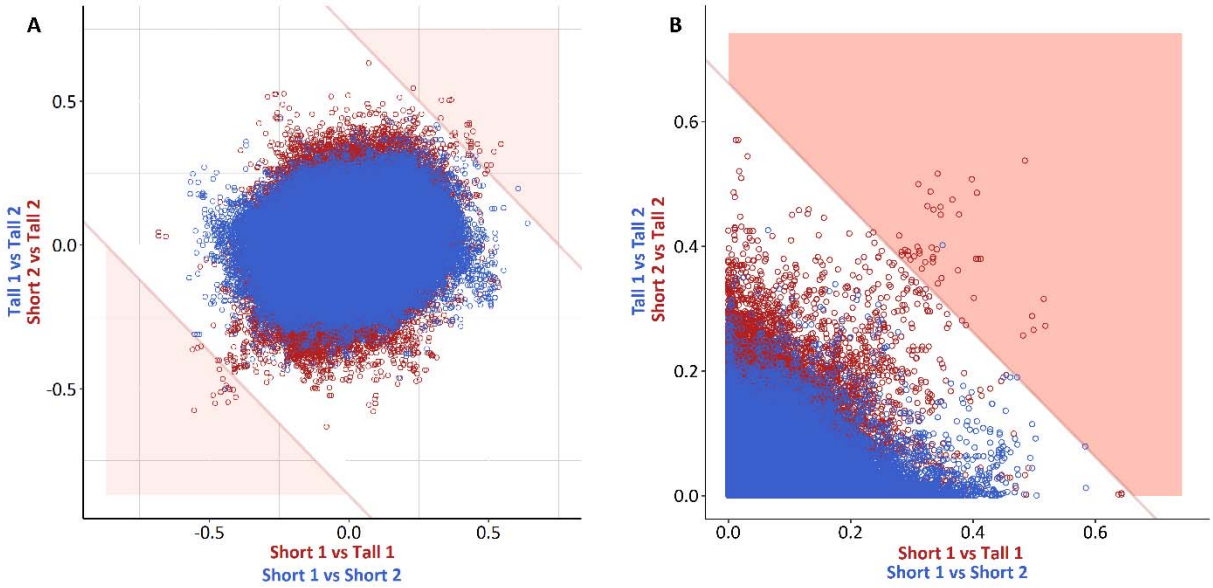

S5: $F_{ST}Sum$ values and the number of markers observed with these values computed between the subpopulations selected in the same (SD) and opposite directions (OD)

F_{ST} *Sum*	SNPs observed between subpopulations selected in		FDRfS	F_{ST} *Sum*	SNPs observed between subpopulations selected in		FDRfS	F_{ST} *Sum*	SNPs observed between subpopulations selected in		FDRfS
	SD	OD			SD	OD			SD	OD	
0	1417796	1421826	0.9972	0.651	4	46	0.0870	0.717	1	25	0.0400
0.01	1104313	1115771	0.9897	0.652	4	46	0.0870	0.718	1	24	0.0417
0.02	400204	415091	0.9641	0.653	4	46	0.0870	0.719	1	23	0.0435
0.03	243600	259984	0.9370	0.654	4	46	0.0870	0.72	1	23	0.0435
0.04	182635	198752	0.9189	0.655	4	45	0.0889	0.721	1	23	0.0435
0.05	142278	159055	0.8945	0.656	4	45	0.0889	0.722	1	23	0.0435
0.06	112868	128888	0.8757	0.657	4	45	0.0889	0.723	1	23	0.0435
0.07	90337	105548	0.8559	0.658	4	45	0.0889	0.724	1	23	0.0435
0.08	72791	87109	0.8356	0.659	4	45	0.0889	0.725	1	23	0.0435
0.09	58794	72032	0.8162	0.66	4	44	0.0909	0.726	1	23	0.0435
0.1	47919	60099	0.7973	0.661	4	44	0.0909	0.727	1	23	0.0435
0.11	39137	50155	0.7803	0.662	2	44	0.0455	0.728	1	23	0.0435
0.12	32127	41814	0.7683	0.663	1	42	0.0238	0.729	1	23	0.0435
0.13	26525	34991	0.7581	0.664	1	42	0.0238	0.73	1	23	0.0435
0.14	21905	29423	0.7445	0.665	1	42	0.0238	0.731	1	22	0.0455
0.15	18173	24779	0.7334	0.666	1	42	0.0238	0.732	1	22	0.0455
0.16	15063	20978	0.7180	0.667	1	42	0.0238	0.733	1	22	0.0455
0.17	12473	17818	0.7000	0.668	1	42	0.0238	0.734	1	22	0.0455
0.18	10368	15116	0.6859	0.669	1	42	0.0238	0.735	1	22	0.0455
0.19	8575	12813	0.6692	0.67	1	41	0.0244	0.736	1	22	0.0455
0.2	7189	10750	0.6687	0.671	1	41	0.0244	0.737	1	21	0.0476
0.21	6061	9106	0.6656	0.672	1	41	0.0244	0.738	1	20	0.0500
0.22	5126	7771	0.6596	0.673	1	41	0.0244	0.739	1	19	0.0526
0.23	4375	6602	0.6627	0.674	1	41	0.0244	0.74	1	19	0.0526
0.24	3633	5611	0.6475	0.675	1	40	0.0250	0.741	1	19	0.0526
0.25	3083	4782	0.6447	0.676	1	40	0.0250	0.742	1	19	0.0526
0.26	2579	4086	0.6312	0.677	1	39	0.0256	0.743	1	19	0.0526
0.27	2161	3477	0.6215	0.678	1	39	0.0256	0.744	1	19	0.0526
0.28	1820	2979	0.6109	0.679	1	39	0.0256	0.745	1	19	0.0526
0.29	1544	2543	0.6072	0.68	1	38	0.0263	0.746	1	19	0.0526
0.3	1304	2188	0.5960	0.681	1	37	0.0270	0.747	1	19	0.0526
0.31	1085	1865	0.5818	0.682	1	37	0.0270	0.748	1	19	0.0526
0.32	909	1561	0.5823	0.683	1	36	0.0278	0.749	1	19	0.0526
0.33	762	1336	0.5704	0.684	1	35	0.0286	0.75	1	19	0.0526
0.34	637	1175	0.5421	0.685	1	35	0.0286	0.751	1	19	0.0526
0.35	551	1034	0.5329	0.686	1	34	0.0294	0.752	1	19	0.0526
0.36	466	901	0.5172	0.687	1	34	0.0294	0.753	0	19	0.0000
0.37	396	780	0.5077	0.688	1	33	0.0303	0.754	0	19	0.0000
0.38	333	683	0.4876	0.689	1	33	0.0303	0.755	0	19	0.0000
0.39	283	605	0.4678	0.69	1	33	0.0303	0.76	0	19	0.0000
0.4	241	527	0.4573	0.691	1	33	0.0303	0.77	0	18	0.0000
0.41	215	483	0.4451	0.692	1	33	0.0303	0.78	0	18	0.0000
0.42	176	436	0.4037	0.693	1	33	0.0303	0.79	0	15	0.0000
0.43	153	391	0.3913	0.694	1	33	0.0303	0.8	0	10	0.0000
0.44	138	363	0.3802	0.695	1	33	0.0303	0.81	0	10	0.0000
0.45	113	327	0.3456	0.696	1	33	0.0303	0.82	0	7	0.0000
0.46	98	298	0.3289	0.697	1	31	0.0323	0.83	0	6	0.0000
0.47	89	267	0.3333	0.698	1	30	0.0333	0.84	0	5	0.0000
0.48	78	241	0.3237	0.699	1	30	0.0333	0.85	0	4	0.0000
0.49	70	215	0.3256	0.7	1	30	0.0333	0.86	0	3	0.0000
0.5	59	198	0.2980	0.701	1	30	0.0333	0.87	0	3	0.0000

0.51	51	188	0.2713	0.702	1	29	0.0345	0.88	0	3	0.0000
0.52	40	178	0.2247	0.703	1	29	0.0345	0.89	0	3	0.0000
0.53	32	157	0.2038	0.704	1	29	0.0345	0.9	0	2	0.0000
0.54	23	142	0.1620	0.705	1	29	0.0345	0.91	0	1	0.0000
0.55	18	134	0.1343	0.706	1	28	0.0357	0.92	0	1	0.0000
0.56	15	125	0.1200	0.707	1	28	0.0357	0.93	0	1	0.0000
0.57	12	113	0.1062	0.708	1	28	0.0357	0.94	0	1	0.0000
0.58	10	107	0.0935	0.709	1	27	0.0370	0.95	0	1	0.0000
0.59	9	99	0.0909	0.71	1	26	0.0385	0.96	0	1	0.0000
0.6	7	92	0.0761	0.711	1	26	0.0385	0.97	0	1	0.0000
0.61	7	86	0.0814	0.712	1	26	0.0385	0.98	0	1	0.0000
0.62	6	83	0.0723	0.713	1	26	0.0385	0.99	0	1	0.0000
0.63	6	72	0.0833	0.714	1	26	0.0385	1	0	1	0.0000
0.64	6	63	0.0952	0.715	1	26	0.0385				
0.65	5	46	0.1087	0.716	1	25	0.0400				

S6: Significance thresholds corresponding to other percentiles of the simulated distribution

Percentile	**Significance threshold**
99th percentile	0.0952
99.9th percentile	0.1277
99.99th percentile	0.1555
99.999th percentile	0.1827
99.9999th percentile	0.2043

S7: Absolute allele frequency differences (AbsAFD) values and the number of SNPs observed with these values computed between the subpopulations selected in the same and opposite directions

Abs AFD	**SNPs observed between subpopulations selected in**		**FDRfS**	**Abs AFD**	**SNPs observed between subpopulations selected in**		**FDRfS**	**Abs AFD**	**SNPs observed between subpopulations selected in**		**FDRfS**
	the same direction (SD)	**opposite directions (OD)**			**SD**	**OD**			**SD**	**OD**	
0	4029092	4029092	1.0000	0.39	3963	6811	0.5819	0.78	6	57	0.1053
0.01	1349787	1353321	0.9974	0.4	3434	6034	0.5691	0.79	6	51	0.1176
0.02	485323	490866	0.9887	0.41	2982	5284	0.5643	0.80	6	46	0.1304
0.03	364245	371265	0.9811	0.42	2571	4667	0.5509	0.81	5	40	0.1250
0.04	312713	320343	0.9762	0.43	2187	4105	0.5328	0.82	5	35	0.1429
0.05	273329	282125	0.9688	0.44	1883	3595	0.5238	0.83	5	34	0.1471
0.06	240504	250277	0.9610	0.45	1610	3135	0.5136	0.84	5	28	0.1786
0.07	212146	223348	0.9498	0.46	1369	2759	0.4962	0.85	4	24	0.1667
0.08	187355	199547	0.9389	0.47	1179	2425	0.4862	0.86	3	22	0.1364
0.09	166014	179002	0.9274	0.48	976	2116	0.4612	0.87	1	18	0.0556
0.1	147328	160900	0.9156	0.49	820	1877	0.4369	0.88	1	17	0.0588
0.11	131038	144737	0.9054	0.5	679	1638	0.4145	0.89	1	16	0.0625
0.12	116706	130343	0.8954	0.51	551	1427	0.3861	0.90	1	14	0.0714
0.13	103839	117425	0.8843	0.52	445	1244	0.3577	0.91	1	13	0.0769
0.14	92437	105670	0.8748	0.53	364	1048	0.3473	0.92	1	11	0.0909
0.15	82509	95231	0.8664	0.54	310	893	0.3471	0.93	1	7	0.1429
0.16	73510	85709	0.8577	0.55	259	756	0.3426	0.94	0	6	0.0000
0.17	65650	77202	0.8504	0.56	222	638	0.3480	0.95	0	5	0.0000
0.18	58555	69483	0.8427	0.57	177	549	0.3224	0.96	0	5	0.0000
0.19	52253	62655	0.8340	0.58	144	471	0.3057	0.97	0	5	0.0000

0.2	46536	56367	0.8256	0.59	124	394	0.3147	0.98	0	3	0.0000
0.21	41382	50780	0.8149	0.6	104	340	0.3059	0.99	0	3	0.0000
0.22	36769	45743	0.8038	0.61	88	291	0.3024	1.00	0	3	0.0000
0.23	32630	41125	0.7934	0.62	74	258	0.2868	1.01	0	2	0.0000
0.24	29002	36997	0.7839	0.63	71	221	0.3213	1.02	0	2	0.0000
0.25	25762	33236	0.7751	0.64	62	195	0.3179	1.03	0	1	0.0000
0.26	22827	29793	0.7662	0.65	54	180	0.3000	1.04	0	1	0.0000
0.27	20141	26734	0.7534	0.66	46	169	0.2722	1.05	0	1	0.0000
0.28	17808	23977	0.7427	0.67	38	150	0.2533	1.06	0	1	0.0000
0.29	15679	21527	0.7283	0.68	33	136	0.2426	1.07	0	1	0.0000
0.3	13851	19268	0.7189	0.69	25	128	0.1953	1.08	0	1	0.0000
0.31	12180	17264	0.7055	0.7	21	112	0.1875	1.09	0	1	0.0000
0.32	10659	15435	0.6906	0.71	19	100	0.1900	1.10	0	1	0.0000
0.33	9312	13827	0.6735	0.72	16	90	0.1778	1.11	0	1	0.0000
0.34	8137	12323	0.6603	0.73	14	87	0.1609	1.12	0	1	0.0000
0.35	7113	10947	0.6498	0.74	10	78	0.1282	1.13	0	0	0.0000
0.36	6202	9742	0.6366	0.75	8	72	0.1111	1.14	0	0	0.0000
0.37	5338	8629	0.6186	0.76	8	70	0.1143	1.15	0	0	0.0000
0.38	4633	7675	0.6036	0.77	7	63	0.1111	1.16	0	0	0.0000

S8: Differentiation along the entire genome expressed by F_{ST} at each SNP marker between the subpopulations selected in opposite directions (A) and the same direction (B) with the significance thresholds based on the 99.9th percentile of the empirical distribution (light purple), based on the 99.99th percentile of the empirical distribution (dark purple) and by the false discovery rate for selection (FDRfS) (yellow).

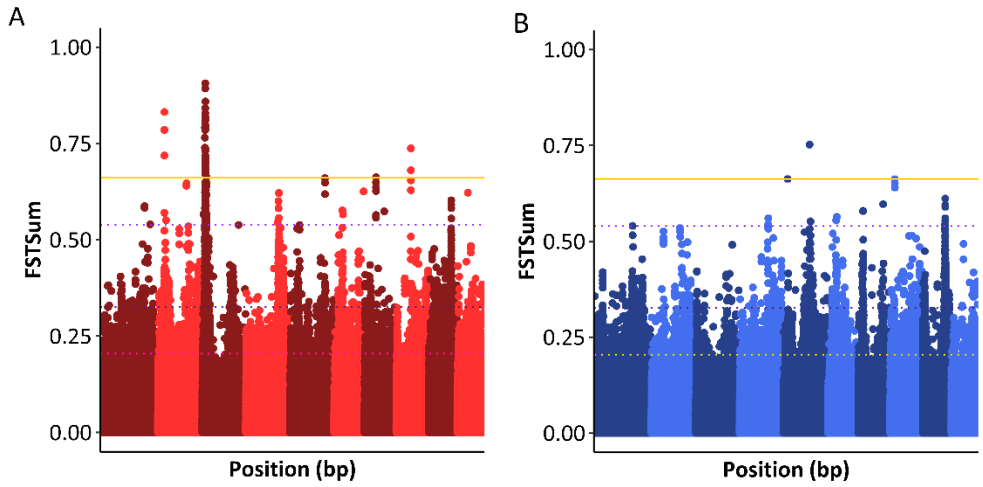

S9: Significant SNP markers and regions with their associated gene models and candidate genes.

Chr	Position (bp)	F_{ST}*Sum* value	Maize gene annotation and candidate gene nearby	Distance to gene (bp)
2	19993292	0.7187	nothing	
2	19993690	0.8316	nothing	
2	19993788	0.7849	nothing	
3	8055976	0.7648	**Zm00001eb121570:** IDP7380	within the coding region
3	8055983	0.7909		
3	8055985	0.7388		
3	9435824	1.0224	**Zm00001eb122210:**	within the coding region

3	9435914	0.9061	No candidate gene associated	
3	9474493	0.8283	**Zm00001eb122220:** No candidate gene associated	within the coding region
3	9529777	0.8925	nothing	
3	9529813	0.8413	nothing	
3	9529816	0.7980	nothing	
3	9529823	0.8103	nothing	
3	9529845	0.7946	nothing	
3	9529863	0.7903	nothing	
3	9544069	0.7926	**Zm00001eb122230:** No candidate gene associated	within the coding region
3	9544090	0.7879		
3	9544092	0.7849		
3	9545220	0.7307		
3	9548992	0.6977	**Zm00001eb122250:** No candidate gene associated	within the coding region
3	9781288	0.7179	**Zm00001eb122280:** pco120183	within the coding region
3	9781314	0.7361		within the coding region
3	9784253	0.7092	**Zm00001eb122290:** No candidate gene associated	within the coding region
3	9784255	0.6966		
3	9784270	0.7150		
3	9792757	0.6828	nothing	
3	9830677	0.7018	**Zm00001eb122300:** No candidate gene associated	within the coding region
3	9909752	0.6876	**Zm00001eb122350:** No candidate gene associated	within the coding region
3	9921856	0.6766	**Zm00001eb122360:** No candidate gene associated	
3	9921871	0.6833		
3	9921927	0.6749		
3	9921995	0.8183		
3	9922080	0.7083		
3	9922083	0.7052		
3	10053938	0.6698	**Zm00001eb122410:** iAA8 - Aux/iAA-transcription factor 8	within the coding region
3	10053961	0.6796		
3	10053964	0.6857		
3	10062671	0.6967		
3	10355793	0.8104	**Zm00001eb122500:** Dwarf1 - dwarf plant1	
3	10355846	0.8589		
3	15011305	0.6630	nothing	
5			**Zm00001eb221820:** impb24 - importin beta24	overlaps with the coding region
7	79405796	0.6624	nothing	
7			**Zm00001eb306380:** pip2e - plasma membrane intrinsic protein2	overlaps with the coding region
8	93026326	0.7371	nothing	
8	93026386	0.6803	nothing	

S10: Detailed overview of gene models within and close to the putatively selected regions

CHR	Start	End	Name	Alias	Description
3	9470819	9476078	Zm00001eb122220	NA	Serinc-domain containing serine and sphingolipid biosynthesis protein
3	9543682	9545931	Zm00001eb122230	NA	Uncharacterized protein
3	9544124	9546235	Zm00001eb122240	NA	UDP-glycosyltransferase 75B1

3	9546098	9555473	Zm00001eb122250	NA	Enhancer of polycomb-like protein
3	9696740	9699326	Zm00001eb122260	NA	Ribosome biogenesis regulatory protein
3	9746003	9777132	Zm00001eb122270	defective kernel5	Embryo defective 2410
3	9779407	9782194	Zm00001eb122280	NA	Uncharacterized protein
3	9783184	9788102	Zm00001eb122290	NA	Syntaxin-32
3	9829261	9831034	Zm00001eb122300	NA	HXXXD-type acyl-transferase family protein
3	9837432	9838607	Zm00001eb122320	NA	BHLH domain-containing protein
3	9843238	9857141	Zm00001eb122340	NA	Kinesin-like protein
3	9908094	9910320	Zm00001eb122350	NA	Alpha/beta-Hydrolases superfamily protein
3	9921652	9923438	Zm00001eb122360	NA	60S ribosomal protein L18A
3	9924317	9927168	Zm00001eb122370	NA	D-aminoacyl-tRNA deacylase
3	9984478	9986791	Zm00001eb122380	NA	ROTUNDIFOLIA like 8
3	9985209	9985860	Zm00001eb122390	NA	Uncharacterized protein
3	10040701	10044498	Zm00001eb122400	NA	RING/U-box superfamily protein
3	10062219	10065595	Zm00001eb122410	Aux/IAA-transcription factor 8	Auxin-responsive protein
3	10072802	10076295	Zm00001eb122420	NA	Serine/threonine protein phosphatase 2A regulatory subunit
3	10121157	10124038	Zm00001eb122440	NA	Protein PGR
3	10161150	10163377	Zm00001eb122450	NA	Uncharacterized protein
3	10164284	10211791	Zm00001eb122460	NA	Pyridoxal phosphate (PLP)-dependent transferase superfamily protein; Aminotransferase class I/classII domain-containing protein
3	10262628	10272956	Zm00001eb122470	glossy13	Glossy13; ABC transporter domain-containing protein
3	10308925	10309311	Zm00001eb122480	NA	Major facilitator superfamily (MFS) profile domain-containing protein
3	10308943	10319637	Zm00001eb122490	NA	Uncharacterized protein
3	10440993	1044334	Zm00001eb122500	dwarf plant1	Dwarf plant1 (GA 3-oxidase 1)
3	10463503	10464262	Zm00001eb122510	NA	Uncharacterized protein
3	10507638	10508780	Zm00001eb122520	bzr6 (BZR-transcription factor 6)	Protein BZR1 homolog (Protein BRASSINAZOLE-RESISTANT 1 homolog)
5	29693525	29695578	Zm00001eb221780	NA	Myb domain protein 15
5	29741878	29756712	Zm00001eb221790	NA	Malate dehydrogenase (EC 1.1.1.37)
5	30046300	30047850	Zm00001eb221810	NA	Protein LIGHT-DEPENDENT SHORT HYPOCOTYLS 3
5	30147389	30180767	Zm00001eb221820	importin beta24	Transportin MOS14
5	30171790	30172570	Zm00001eb221830	NA	Uncharacterized protein
5	30322455	30325916	Zm00001eb221840	NA	DYW domain-containing protein
5	30327060	30333792	Zm00001eb221850	NA	Methyltransferase (EC 2.1.1.-)
5	30436204	30452215	Zm00001eb221860	NA	Serine/threonine protein phosphatase 2A regulatory subunit B''alpha; PP2A regulatory subunit B'' EF-hand domain-containing

					protein
5	30569037	30574617	Zm00001eb221870	NA	Casein kinase 1-like protein 6; Protein kinase domain-containing protein
5	30569279	30570211	Zm00001eb221880	NA	Uncharacterized protein
7	42250227	42251850	Zm00001eb306350	beta expansin4	Beta expansin4 (Beta-expansin 4)
7	42356910	42373012	Zm00001eb306360	NA	SUPPRESSOR OF ABI3-5
7	42530874	42533448	Zm00001eb306370	NA	60S ribosomal protein L44
7	42614221	42617867	Zm00001eb306380	NA	Aquaporin PIP2-1 (Plasma membrane intrinsic protein 2-1) (ZmPIP2-1) (ZmPIP2;1); Uncharacterized protein
7	42663460	42664219	Zm00001eb306390	NA	Uncharacterized protein
7	42734578	42736049	Zm00001eb306400	NA	Aquaporin PIP2-6 (Plasma membrane intrinsic protein 2-6) (ZmPIP2-6) (ZmPIP2;6); Uncharacterized protein
7	42940009	43002780	Zm00001eb306410	NA	phosphoglucomutase (alpha-D-glucose-1,6-bisphosphate-dependent) (EC 5.4.2.2)

S11: Average haplotype block size and number of blocks in the 39 randomly selected regions across the entire genome which had the same marker density (3000 markers) and the same length (1.0217 Mb) like the region on chromosome 3 from 9.411 to 10.423 Mb.

Chr	Start	End	Size in bp	MD	Average block size in bp				Number of blocks			
					Short 1 (S1)	Short 2 (S2)	Tall 1 (T1)	Tall 2 (T2)	S1	S2	T1	T2
1	4656255	5673715	1017456	3001	168.38	192.03	152.18	181.30	48	58	49	53
1	4657515	5675008	1017542	3001	172.43	192.07	151.11	142.99	61	68	65	70
1	136651493	137669028	1017508	3001	167.00	188.48	163.87	146.39	57	65	61	70
1	136651521	137669044	1017451	3001	232.23	236.53	280.61	240.68	40	36	36	38
1	141324802	142342317	1017529	3001	197.88	220.78	237.32	277.22	41	41	31	37
1	299047457	300064908	1017515	3001	230.58	208.98	203.65	156.20	55	47	55	56
1	299916606	300934135	1017508	3001	219.79	177.62	175.16	157.65	53	50	58	57
2	211868837	212886299	1017460	3001	321.03	292.52	253.09	377.07	33	33	34	29
3	209603974	210621427	1017493	3001	431.55	616.71	718.93	616.89	22	17	15	19
3	215324449	216341997	1017535	3001	409.52	633.83	649.58	644.14	21	12	12	14
3	226284531	227301995	1017523	3001	445.88	725.27	943.10	574.50	16	11	10	12
4	5894188	6911719	1017515	3001	849.17	1381.00	1066.50	1142.20	6	3	6	5
4	178073590	179091042	1017462	3001	875.88	740.90	587.95	487.78	8	10	19	18
4	189758118	190775592	1017453	3001	419.25	592.39	362.86	426.57	28	18	29	30
4	248403619	249421075	1017548	3001	298.69	326.55	273.33	274.40	26	29	30	30
5	11579536	12596999	1017464	3001	340.62	641.70	325.09	354.88	29	10	32	24
5	190705257	191722765	1017531	3001	197.82	248.51	261.66	215.86	38	35	32	35
5	205704485	206721937	1017452	3001	329.77	398.82	243.42	274.54	26	22	24	26
6	156935769	157953269	1017474	3001	198.81	182.06	193.84	183.47	43	34	31	36
6	172123748	173141295	1017456	3001	169.51	178.05	161.30	174.98	57	56	56	66
6	177840537	178858074	1017463	3001	222.46	255.28	192.97	223.12	37	36	37	42
7	135802410	136819947	1017508	3001	493.76	588.22	432.61	523.24	17	9	18	17
7	135802513	136819970	1017452	3001	485.39	626.85	310.09	659.57	18	13	23	14

7	152794989	153812490	1017500	3001	447.40	434.86	597.31	497.47	15	14	13	17
7	173575391	174592938	1017547	3001	407.83	399.71	469.30	387.68	18	17	20	19
7	177034864	178052383	1017537	3001	316.96	345.17	363.70	289.46	26	24	23	28
7	177500666	178518212	1017537	3001	276.34	182.79	224.03	200.12	35	47	39	43
8	157927948	158945468	1017457	3001	275.66	196.18	208.02	176.82	41	49	44	45
8	174898862	175916406	1017501	3001	358.54	266.38	241.31	222.70	24	29	32	37
9	12444447	13461916	1017547	3001	2644.00	1971.50	2661.00	2645.00	1	2	1	1
9	12444505	13461971	1017519	3001	350.53	479.43	400.67	509.00	17	14	15	15
9	134126843	135144313	1017546	3001	269.13	355.93	283.50	220.69	30	28	28	35
9	134132144	135149684	1017520	3001	973.78	586.07	598.20	933.22	9	14	15	9
9	151992522	153010067	1017544	3001	346.94	389.26	379.84	290.59	16	23	25	32
10	4656255	5673715	1017469	3001	137.72	137.83	125.36	116.89	54	60	58	64
10	4657515	5675008	1017466	3001	149.33	156.16	147.72	126.95	52	50	54	57
10	136651493	137669028	1017470	3001	261.16	318.96	326.96	243.13	32	25	26	31
10	136651521	137669044	1017540	3001	288.21	310.84	339.34	232.37	33	31	32	38
10	141324802	142342317	1017545	3001	328.13	290.68	244.97	237.84	23	34	32	38

S12: Average haplotype block size and number of blocks in the 39 randomly selected regions across the entire genome which had the same marker density (3000 markers) and the same length (1.0217 Mb) as the region on chromosome 3 from 9.411 to 10.423 Mb.

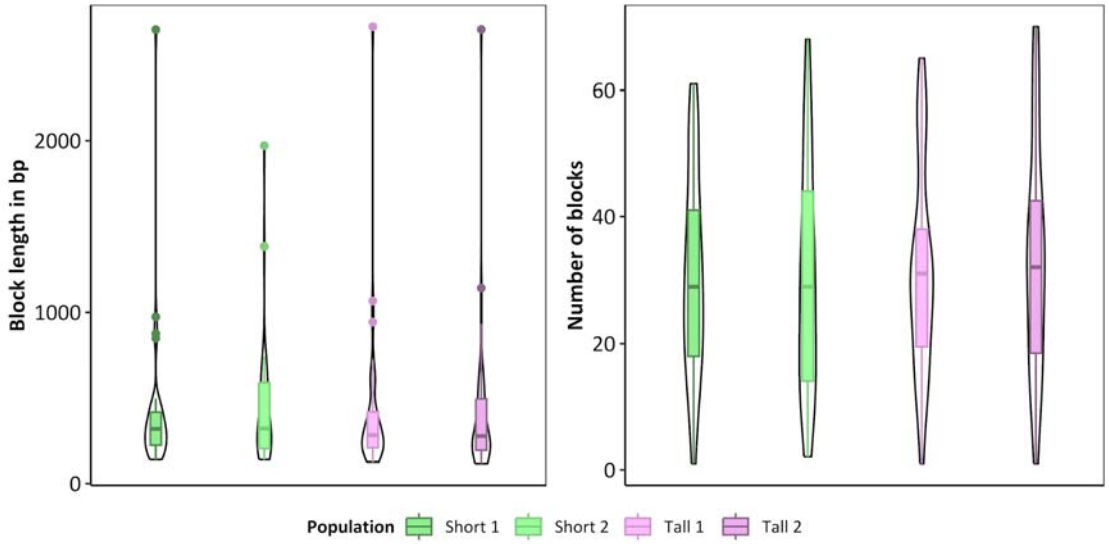

S15: LD decay plot across the entire genome for the four subpopulations based on 10,000 randomly sampled SNPs per chromosome.

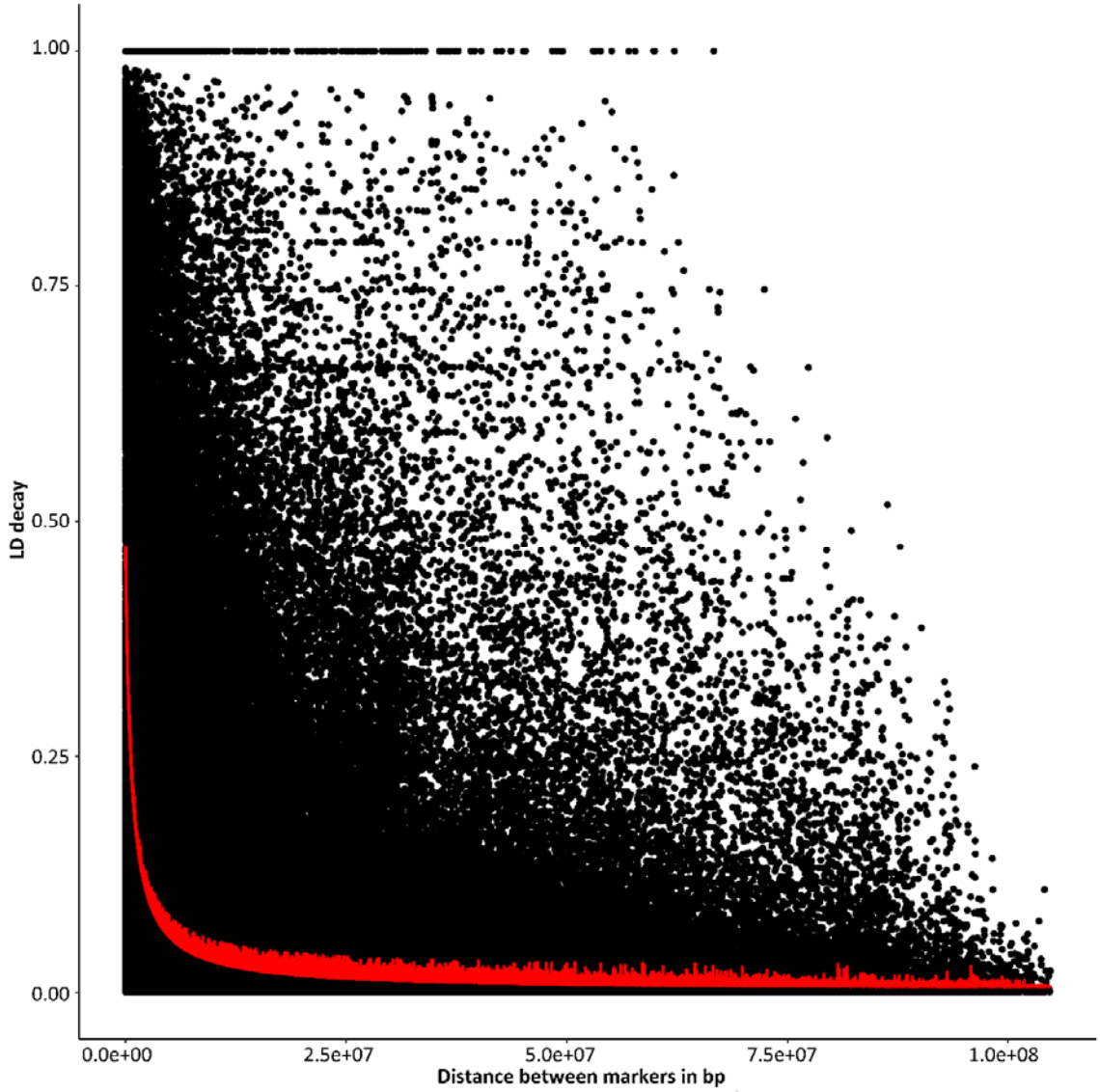

S14: Haplotype blocks calculated in a randomly selected region on chromosome 1 from 299.05 Mb to 300.07 Mb, which had the same marker density (3000 markers) and the same length (1.0217 Mb) as the region on chromosome 3 from 9.411 to 10.423 Mb.

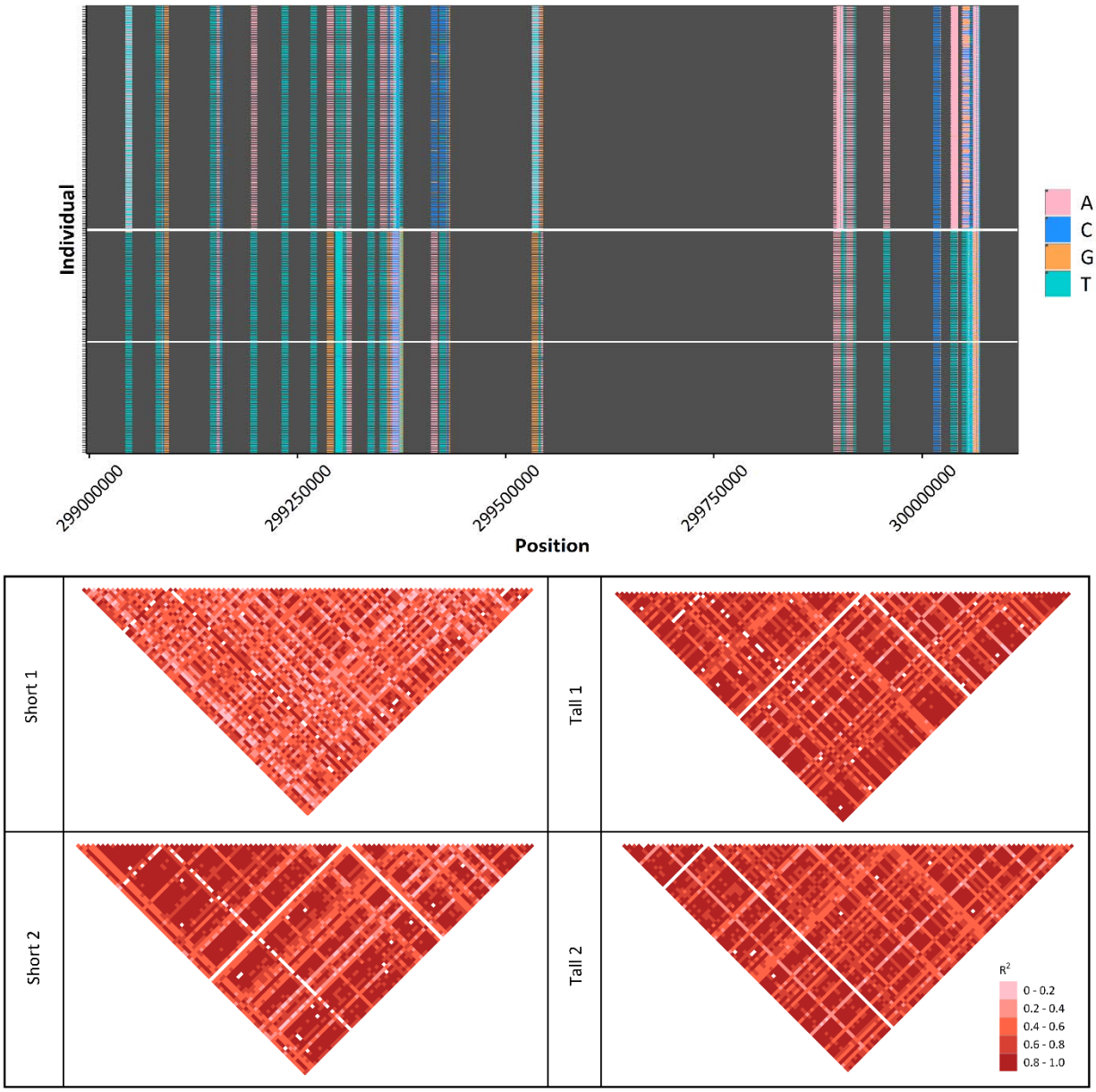

S15: Haplotype blocks calculated in a randomly selected region on chromosome 7 from 177.04 Mb to 178.05 Mb, which had the same marker density (3000 markers) and the same length (1.0217 Mb) as the region on chromosome 3 from 9.411 to 10.423 Mb.

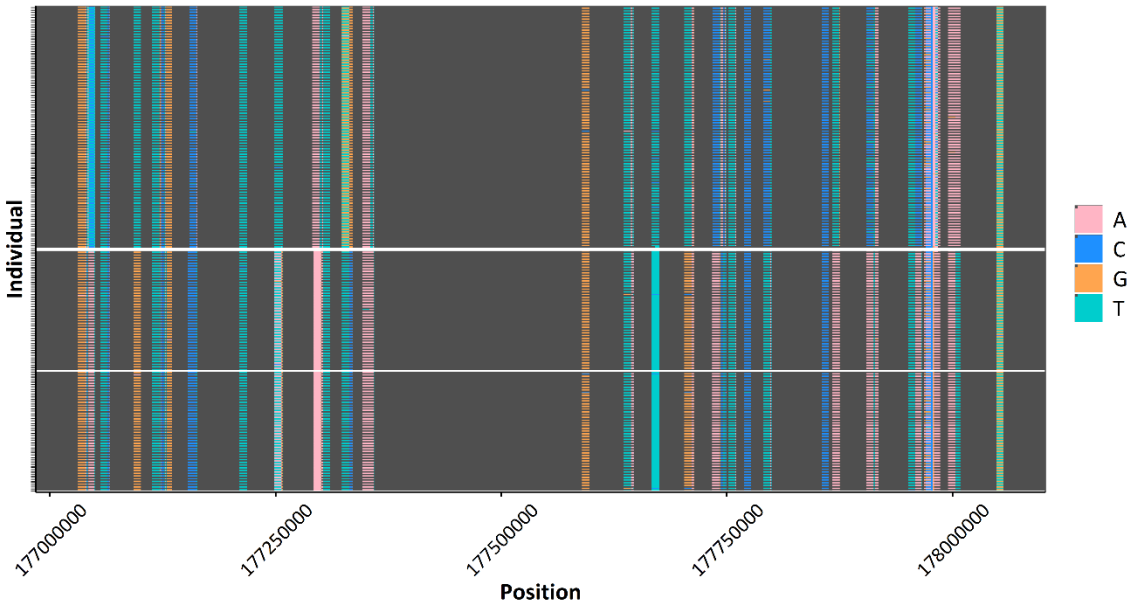
Individual
A
C
G
T
177000000
177250000
177500000
177750000
178000000
Position

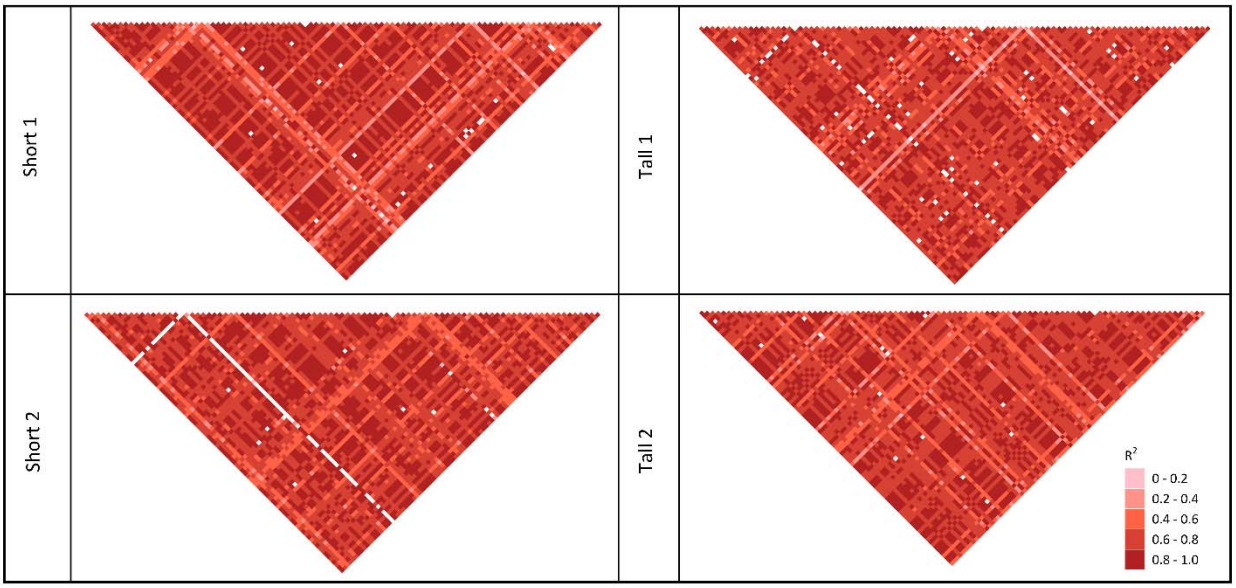
Short 1
Tall 1
Short 2
Tall 2
R²
0 - 0.2
0.2 - 0.4
0.4 - 0.6
0.6 - 0.8
0.8 - 1.0